Energy Advances

ROYAL SOCIETY OF CHEMISTRY

REVIEW ARTICLE

View Article Online
View Journal | View Issue

Cite this: *Energy Adv.*, 2024, 3, 30

A review on the advancements of graphitic carbon nitride-based photoelectrodes for photoelectrochemical water splitting

Merin Joseph, [a] Mohit Kumar, [cd] Suja Haridas, *[ab] Challapalli Subrahmanyam *[c] and Sebastian Nybin Remello[ab]

Received 13th October 2023,
Accepted 6th December 2023

DOI: 10.1039/d3ya00506b

rsc.li/energy-advances

Photoelectrochemical water splitting has been envisaged as a promising green technology for efficient solar-to-fuel conversion. Graphitic carbon nitride (g-C_3N_4) demands prime focus among the emerging class of potential 2D materials for energy harvesting and storage on account of its high chemical/thermal stability and metal-free nature. The unique characteristics of the material enable its application as both a photocathode and photoanode. However, the low photocurrent density of pristine g-C_3N_4 curbs its possible commercial application. Considerable attempts to modify the electrodes *via* nanostructuring, heteroatom doping, heterojunction formation, and other methods are in progress. The current review offers insights into the potential and limitations of g-C_3N_4 as a photoanodic/cathodic material.

1. Introduction

The rapidly growing energy demands have challenged the scientific society to come up with clean, renewable, and sustainable energy sources. However, clean renewable resources, such as solar, tidal, wind, and geothermal energy, have their own sets of limitations that hamper the replacement of the current fossil fuel-based non-renewable resources.[1] In this scenario, solar energy utilisation remains the most promising

[a] *Department of Applied Chemistry, Cochin University of Science and Technology, Kochi, Kerala, 682022, India. E-mail: sujaharidas@cusat.ac.in*
[b] *Inter University Centre for Nanomaterials and Devices, Cochin University of Science and Technology, Kochi, Kerala, India*
[c] *Department of Chemistry, Indian Institute of Technology Hyderabad, Hyderabad, Telangana, 502285, India. E-mail: csubbu@iith.ac.in*
[d] *Department of Chemistry and Biochemistry, School of Science Computing and Engineering, Swinburne University of Technology, Hawthorn, VIC-3122, Australia*

Merin Joseph

Merin Joseph obtained her postgraduate degree in Chemistry from St. George's College, Mahatma Gandhi University, Kerala. Since July 2018, she has been a PhD student under the guidance of Dr Suja Haridas and the co-guidance of Dr Sebastian Nybin Remello in the Department of Applied Chemistry, Cochin University of Science and Technology. Her research focuses on the energy harvesting and environmental remediation based on graphitic carbon nitride hybrids.

Mohit Kumar

Mohit Kumar studied chemistry at the Indian Institute of Technology Hyderabad, India, where he obtained his postgraduate degree in Chemistry. Since May 2020, he has been a joint PhD student in the IITH-SUT joint doctoral programme under the guidance of Challapalli Subrahmanyam in the Department of Chemistry at the Indian Institute of Technology Hyderabad, TN, India, and the Chenghua Sun, School of Science, Engineering and Technology, Swinburne University of Technology, VIC, Australia. His research focuses on the development of novel Cu-based semiconducting photocathode configurations for solar water splitting.

approach to provide a sustainable solution to the energy crisis. Despite the abundant and inexhaustible solar energy incident on the earth's surface, the average utilisation remains meagre. The core requirement for solar energy utilisation is the mild conditions for the operational feasibility of reactions allowing for the fine-tuning of the selectivity.[2,3] In conjunction with energy generation, energy storage is also of crucial significance, with electrochemical and chemical energy storage[4,5] being equally explored in this domain. Efficient conversion of solar energy into chemical energy is as momentous and challenging as direct solar-to-electric conversion. Hydrogen is regarded as a potential clean fuel with zero carbon emission for the future, and sustainable H_2 generation demands prime priority. Of several available technologies for H_2 production, photoelectrochemical (PEC) water splitting has gained popularity owing to its relative simplicity and environmental benignity.[1–3,6–9] In comparison with photocatalytic water splitting, PEC benefits from the generation of H_2 and O_2 over separate electrodes, avoiding gas mixing and back reactions. The external bias applied in PEC significantly allows for charge separation and migration, achieving high efficiency as compared to photocatalytic water splitting. Photoelectrocatalysis has been applied in chemical synthesis and nitrogen reduction in addition to water splitting.[10,11]

After the initial design of PEC water splitting by Fujishima and Honda,[12] the process has received much attention in the realm of solar energy conversion and storage revolution.[13] A typical process in a PEC cell involves the light-assisted generation of voltage by photoactive semiconducting electrodes and the mobilization of charge carriers to bring forth water splitting. Efficient PEC water splitting entails materials complying with various criteria, including suitable band edge positions, an appreciable absorption of the solar spectrum, effective charge separation, high hydrolytic stability and photostability, and cost-effectiveness.[1–3,6,13,14] Numerous semiconductor materials have been employed for efficient PEC water splitting.[15–26] However, due to the complex electrode kinetics, fast exciton recombination, large over potential, and photostability of materials, achievable solar-to-hydrogen conversion efficiencies (STH) remain too low, thus limiting the commercialisation of PEC water splitting.

Graphitic carbon nitride (g-C_3N_4), a metal-free polymeric semiconductor material, has aroused global interest as a multifunctional material for energy harvesting and storage.[27,28] Although the material was known for a long time,[29] Wang *et al.* first reported the photocatalytic activity of g-C_3N_4 in 2009.[30] Ever since then, we have seen many reports on the profuse applications of g-C_3N_4 regarding photocatalytic H_2 production,[31–33] pollutant degradation,[34,35] CO_2 reduction,[36,37] *etc.* The suitable electronic band structure, visible light absorption capability, non-toxicity, and easy synthesis from low-cost precursors render g-C_3N_4 an ideal photoelectrode material for energy harvesting. The photocurrent responses of carbon nitride solids were first reported by Zhang *et al.*[38] in 2010, paving a new path for PEC applications.[39] Several reports covering various aspects of g-C_3N_4-based PEC water splitting are available in the literature,[39–45] most of which are primarily focused on film fabrication strategies. In this review, we provide a concise depiction of the basic

Suja Haridas

Suja Haridas obtained her PhD from Department of Applied Chemistry, Cochin University of Science and Technology in 2002. She is currently an Associate Professor, Department of Applied Chemistry, CUSAT, Kerala. Her research interests include heterogeneous catalysis and photocatalysis as well as 2D materials for energy harvesting, storage and membrane technology.

Challapalli Subrahmanyam

Challapalli Subrahmanyam obtained his PhD in Chemistry from the Indian Institute of Technology, Madras, in 2003. From 2003 to 2007, he was a postdoctoral fellow in the École Polytechnique Fédérale de Lausanne, Switzerland. He started his academic career as an Assistant Professor at the National Institute of Technology Trichy, India. In 2009, he moved to the Indian Institute of Technology, Hyderabad, as an Assistant Professor, where he is currently a professor of Chemistry. His research focuses on nanomaterials for solar energy harvesting and environmental remediation.

Sebastian Nybin Remello

Dr Sebastian Nybin Remello joined the Department of Chemistry as an Assistant Professor in 2017. He received his PhD (Applied Chemistry) in 2015 from the Department of Applied Chemistry, Tokyo Metropolitan University, Tokyo. From 2015–2017, he worked as a postdoctoral research fellow at the Center for Artificial Photosynthesis, Tokyo Metropolitan University. His primary area of research is the development of chemical architectures for artificial photosynthesis based on metal porphyrins and metal–organic frameworks.

principles of photoelectrochemical water splitting. A brief recap of the potential of g-C_3N_4 as a photo(electrocatalyst) and the various electrode fabrication strategies are provided. The focus here is an in-depth overview of the prevailing status of g-C_3N_4-based photocathodic and photoanodic materials for PEC water splitting. The prospects and challenges are highlighted in the concluding section.

1.1 Hydrogen economy

The development of a hydrogen economy is mankind's finest opportunity for a sustainable energy future considering the rising expense of fossil fuels and concerns about energy security and environmental safety.[46] The hydrogen economy refers to an industrial system where electricity and hydrogen are the two universal energy carriers.[47] In recent decades, there has been a notable surge in interest in hydrogen as a potential energy carrier for a sustainable future. With a low heating value, hydrogen combustion releases more energy than any other fuel when compared mass-wise. Presently, the reforming of fossil fuels accounts for 98% of the annual output of H_2, which is about 0.1 Gton.[48] The most significant advantage of using hydrogen is that when it burns with oxygen, it generates heat and water, unlike fossil fuels, which release carbon dioxide.[49] A 'low-carbon future' will arise from the development of the hydrogen economy. This will lower greenhouse gas emissions globally, which will mitigate their detrimental effects on the climate. As the hydrogen economy progresses, 'green' hydrogen is perhaps the most envisaged form of hydrogen. Hydrogen produced by electrolyzing water using renewable solar energy is green hydrogen, which has zero carbon emissions.[50,51] Despite making up a very small portion of the energy output at the moment, H_2 generation from renewable resources has enormous potential to cover the world's energy needs without having a negative environmental impact.[46] Since the costs of these technologies are still too expensive in comparison to traditional fossil fuel-based technologies, their real-time deployment will require both considerable technology advancements and cost reductions. Innovations in technology are particularly required in the areas of storage, transportation, carbon capture and the low-efficiency hydrogen generation from renewable sources.[49]

1.2 Basics of PEC water splitting

Solar-assisted PEC water splitting is contemplated as a promising approach for sustainable energy production. The basic principle of PEC water splitting involves hydrogen generation utilising solar energy and is aided by an external bias between the semiconductor photoelectrode and a counter electrode in the presence of a suitable electrolyte. The external bias enables the slow kinetics to be overcome and drives the reaction at a desired rate/current density.[52] PEC water splitting is mainly comprised of two half-reactions, water oxidation or oxygen evolution reaction (OER) at the anode and water reduction or hydrogen evolution reaction (HER) at the cathode. Overall, water splitting can be represented as follows: water splitting is an energy-uphill process with a ΔG value of 237 kJ mol^{-1}, rendering it thermodynamically unfavourable.[53] The feasibility of the reaction demands a minimum energy requirement of 1.23 eV.[41] Therefore, the semiconductor photoelectrode should be able to absorb light energy equivalent to or greater than 1.23 V and subsequently generate electron–hole pairs. In order to initiate the overall water splitting, the valence band (VB) maximum of the photocatalyst should be more positive than the water oxidation potential (E^0_{ox} = 1.23 eV at pH 0), and the conduction band (CB) minimum should be more negative than the hydrogen evolution potential (E^0_{red} = 0 eV at pH 0).[2,54] Thus, the wavelength employed, along with the band edge positions of the catalyst, plays a critical role in deciding the efficiency of overall water splitting. The photoinduced physical and chemical processes involved include light absorption, charge separation and migration, charge injection and the corresponding chemical reactions at the electrode.[8,13,26] The efficiency of the process is heavily reliant on the charge transfer at the electrode/electrolyte interface. The electrode materials, depending on their nature, fall under the categories of photoanodes or photocathodes. The electrodes perform the dual roles of light-absorbing antennae promoting electron–hole generation, and active sites for H_2/O_2 evolution. Generally, n-type semiconductors are employed as photoanodes with the Fermi level being closer to the CB minimum. Photocathodes are usually made of p-type semiconductors, with their Fermi level being closer to the VB maximum. When immersed in an electrolyte, there occurs a shift in the Fermi level resulting in the formation of an electric field and a consequent band bending. In the case of n-type semiconductors, we have an upward bending while a downward bending is observed for p-type materials.[38–42] In short, the transfer of electrons to the electrolyte by a p-type semiconductor generates a cathodic photocurrent, while an anodic photocurrent is produced when holes are received by the electrolyte aided by an n-type semiconductor.[53] The electrons generated at the CB of the photocathode directly migrate to the electrode surface, reducing H^+ to H_2, while holes are transported to the anode for water oxidation.[40,41,52,53,55] In the case of the photoanodes, oxygen is evolved due to direct water oxidation by holes. The electrons generated at the anode are directed to the cathode *via* an external circuit. H^+ migrates to the cathode to be eventually reduced to H_2.[8,40,52,53] During the charge migration process, overpotential results from the energy losses occurring when electrons migrate through the external circuit and holes through the space charge region.

$$\text{OER: } 2H_2O \rightarrow O_2 + 4H^+ + 4e^- \quad E^0_{ox} = 1.23\ \text{V} \tag{1}$$

$$\text{HER: } 4H^+ + 4e^- \rightarrow 2H_2 \quad E^0_{red} = 0\ \text{V} \tag{2}$$

$$2H_2O \rightarrow O_2 + 2H_2$$

The general device setup consists of a photoelectrode (cathode/anode), a counter electrode (usually platinum), a suitable electrolyte, and a wire completing the circuit. Semiconductor PEC water splitting may be achieved *via* single or coupled

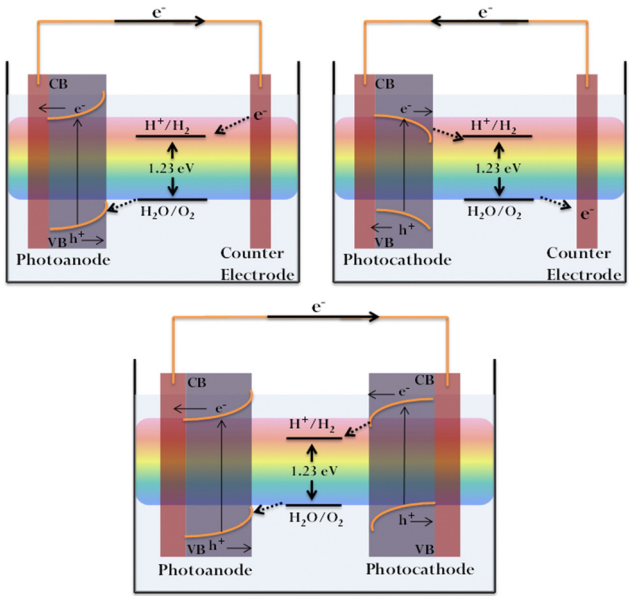

Fig. 1 Schematic representation of PEC water-splitting cells with single and coupled photosystems.

photosystems. In the former case, either the anode or cathode is photoactive, with Pt being the traditional commonly used counter electrode. For the coupled (tandem) photosystems, n- and p-type semiconductors are used as the anode and cathode, respectively (Fig. 1).[55]

1.3 Relevant challenges and attempts for improved PEC performance

The semiconducting photoelectrodes are the vital constituents of a PEC system. A flawless photoelectrode material should meet several requirements, including a low band gap, efficient charge carrier utilization, low overpotential, wide solar spectrum harvesting, excellent stability for extended operation, and facile low-cost fabrication to enable commercialisation. The search is still ongoing to explore new photoelectrode materials exhibiting sustainable PEC performance.[56,57] Recently, several semiconductor materials have been acclaimed as effective photoelectrodes, including oxides, nitrides and sulphides such as TiO_2, $BiVO_4$, WO_3, Fe_2O_3, ZnO, Ta_3N_5, g-C_3N_4, MoS_2, WS_2, *etc.*[15–20,23–26,58,59] Nevertheless, none of them fulfils the requirements for large-scale synthesis and hydrogen generation. The efficiency of hydrogen evolution is dependent on the characteristics of the semiconductor material, including its specific surface area, surface planes, morphology, and optical qualities. The photocatalyst's light absorption range is a property of the semiconductor band gap, whereas the viability for simultaneous water oxidation and reduction is reliant on the conduction and valence band positions.[2] On the other hand, if the material exhibits optimum photocurrent densities, photocorrosion-related stability problems will prevent it from performing for industrial-scale applicability. Unresolved issues including limited catalyst stability and inadequate efficiency are related to the physicochemical characteristics of the semiconductor material.

The fabrication of novel materials and the improvisation of current photocatalyst materials through structural and chemical modifications will enable the large-scale generation of hydrogen from solar energy in an efficient manner.[2] Some of the key design strategies that can be employed to improve the overall performance of the photoelectrodes are listed here.

- The construction of heterojunctions is one of the most frequently utilized techniques for averting charge recombination. A relative shift in band position may be seen when two semiconductors with thermodynamically matched band structures come into contact, causing the band to bend at the interface. By combining a narrow band gap semiconductor with a broad band gap scaffold, light absorption could be enhanced in addition to the internal electric field that improves the charge separation efficiency.[60,61]
- PEC performance has been successfully boosted by tuning the semiconductor materials into several morphologies, including nano-rods/wires, nano-flakes, nanotubes, and nano-porous structures. The condensed material geometry provides a shortcut for the charge transport process in addition to having an accessible area for electrolyte interaction.[60,62,63]
- Heteroatom doping, as demonstrated by theoretical and experimental research, can concurrently improve electrical and light absorption characteristics by generating shallow donor and/or acceptor levels.[6] While employing this tactic, some cases have reported increased donor density and conductivity, while other cases have succeeded in modifying the band gap or even the band structure. However, controlled doping remains challenging.[60,64,65]
- One effective way to raise the photovoltage is to deposit passivation overlayers, which are either a wide band gap semiconductor coating or a layer of extremely thin, comparatively insulating metal oxide. It is used in hematite photoanodes more frequently, which triggers band bending, boosts photovoltage and decreases onset potential.[66]
- The photocorrosion of semiconductor materials, which happens when photogenerated charges drive the material self-oxidation (or reduction) instead of the water-splitting reaction, is one of the major causes of instability in PEC devices.[67] Apart from photocorrosion, there are additional variables that contribute to the instability of PEC water-splitting devices, which are associated with the interfaces between the electrolytes and semiconductor catalysts. Finding materials that are inherently resistant to corrosion remains a potential milestone and is one way to attain high stability; another is to use protective layers that can physically separate the semiconductor materials from the electrolyte. PEC device stability may be impacted by electrolyte conditions (pH, for example); adjusting the electrolyte composition and controlling the dissolution reaction during PEC operation can also help in the stable operation of PEC devices.[6]
- An approach that shows promise for addressing problems with single or heterojunction PEC devices is tandem cell configuration. PEC systems can offer higher STH by harvesting a broader solar spectrum in tandem cell configuration. Photoanode/photocathode (PEC/PEC) and photoelectrode/photovoltaic

(PEC/PV) tandem cells are the two primary types of tandem cell configuration. These tandem dual-absorber devices can maximize the amount of solar energy absorbed while also producing a strong driving force for self-driven solar water splitting. Sunlight first passes through the n-type semiconductor and then the p-type semiconductor in a PEC/PEC tandem cell. The top electrode, the photoanode, absorbs photons with shorter wavelengths in the solar spectrum. The bottom electrode, the photocathode, transmits and collects the remaining photons with longer wavelengths. Thermodynamically, two semiconductors with smaller band gaps can be selected in preference to a single photoelectrode since each photoelectrode only needs to supply a portion of the total potential for water splitting; yet, their stability remains a major concern when in direct contact with electrolytes. A voltage-biased PEC device with an integrated PV device constitutes a PEC/PV tandem cell. The semiconductor material's minority carriers in the PEC photoelectrodes in this configuration take part in the water redox reaction, which happens at the semiconductor–electrolyte junction. When there is insufficient power produced by the minority carriers, solar cells can sustain an operation. Like the PEC/PEC arrangement, light serves as the only energy input for the entire system.[11,68–70]

1.4 g-C_3N_4 as a potential water-splitting photo(electro)catalyst

g-C_3N_4 has a layered graphite-like structure consisting of tri-*s*-triazine units (Fig. 2). The simplistic synthesis route from low-cost precursors, chemical/thermal stability, non-toxicity, and biocompatibility have contributed to the wide interest in the material.

With the VB and CB positions being favourable for both water oxidation and reduction potentials, g-C_3N_4 has attracted great interest as a photo(electro)catalyst. Moreover, g-C_3N_4 shows resistance to photocorrosion.[71] However, the inherent activity is restricted by the limited visible light sensitivity, low surface area, poor electronic conductivity and fast electron–hole recombination. Considerable effort has been directed towards enhancing the performance by lengthening the exciton diffusion length to prevent charge recombination at grain boundaries. Tuning the electronic structure *via* heteroatom doping (metal/non-metal) can alter the absorption edge, enhancing the visible light sensitivity.[72–76] Non-metal species substituting

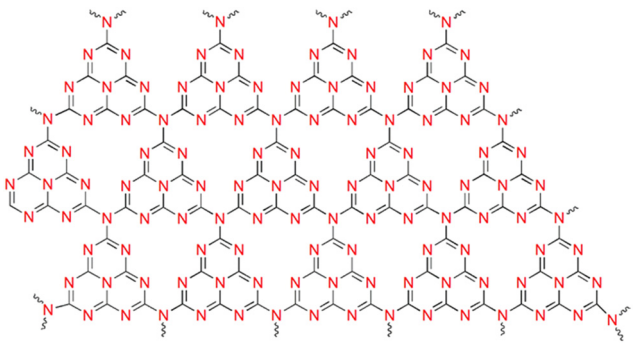

Fig. 2 Schematic illustration of g-C_3N_4 containing tris-*s*-triazine units.

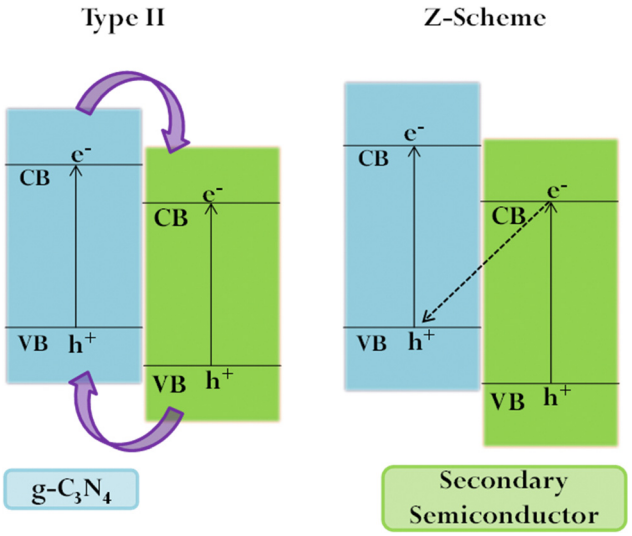

Fig. 3 A graphic illustration of type II and Z-scheme heterojunctions.

carbon and nitrogen in the framework promote charge separation and migration, while metal atoms are substituted in interstitial spaces, thereby introducing defect sites and additional atomic orbitals, which in turn alter the absorption edge.[74,77,78] It needs to be mentioned that excessive doping retards PEC performance by providing sites for charge recombination and triggering side reactions.[79] Creating an efficient heterojunction enables the fast migration of charges at the interface, prolonging the exciton lifetime.[80] The most commonly used ones are Z-scheme and Type II heterojunctions (Fig. 3), which achieve efficient separation of photogenerated electrons and holes, ensuring sustainability. the order of deposition plays a major role in deciding the electron flow and the type of heterojunction formed.[81] As compared to nanoparticles, ordered nanoarrays have been found to promote charge migration, inhibiting recombination at grain boundaries.[41,82,83] Morphological and crystalline factors are also quite crucial in deciding the band gap and charge separation.[53,84,85] The introduction of localised surface plasmon resonance also enhances PEC efficiency.[86–89] It has been reported that combining g-C_3N_4 with other carbon compounds and dye sensitization increases its activity.[90–92]

2. Electrode fabrication strategies

The fabrication of thin films of g-C_3N_4 is a salient step in PEC water splitting. One of the major factors affecting the PEC application of g-C_3N_4 is the difficulty encountered in fabricating uniform high-quality films on the conductive substrate.[44,52] The formation of thin and uniform films of g-C_3N_4 is difficult because of its poor dispersibility/solubility in most of the solvents and subsequent aggregation leads to cracks and non-homogeneous film. Poor adhesive forces between g-C_3N_4 also contribute to the inhomogeneous microstructures of the photoelectrodes leading to a low photocurrent density. There are two types of methods for thin film fabrication: top-down and bottom-up. The top-down approaches to film fabrication

include drop casting,[89,93–100] spin coating,[101–105] dip coating,[106] spray coating,[107] vacuum filtration,[108–112] electrospinning,[113–115] doctor blade,[116,117] *etc.* It is exceedingly difficult to create a uniform and stable slurry or sol of g-C_3N_4 while employing top-down techniques, which often leads to massive aggregations of g-C_3N_4 and cracks in the film as well as the interface between the film and substrate. As a result, PEC performance is frequently low in such top-down manufactured g-C_3N_4 film photoelectrodes.[39] The casting of g-C_3N_4 embedded in a conductive polymer matrix improves charge transport and casting homogeneity.[118]

Several advanced bottom-up approaches have been adopted to enhance the PEC performance of the photoelectrodes by achieving high-quality g-C_3N_4 films. These techniques favour the formation of uniform micro-structured films with intimate contact with the substrate, thereby facilitating smooth charge transfer. The bottom-up approach also enables to mitigate the problem of poor dispersibility of g-C_3N_4. Electrochemical deposition, a commonly used bottom-up approach can be categorised into electrophoretic deposition[119–121] and electrodeposition.[122–124] Electrophoretic deposition is achieved by holding the substrates at the positive and negative potential in a dispersion of exfoliated g-C_3N_4.[119] The strategy avoids high-temperature operation, enabling deposition on thermally unstable substrates like carbon paper and nickel foam, which is essential for flexible film fabrication. Thermal vapour condensation (TVC) involves the direct vaporisation of the solid precursors and deposition as a thin film over the substrate and subsequent polymerisation under controlled thermal conditions[125–137] quite similar to the chemical vapour deposition (CVD) technique. The careful temperature control enables the fine-tuning of the morphological characteristics and microstructure of g-C_3N_4 films. The major advantage of TVC is the non-requirement of sophisticated instrumentation. However, precursors like urea, thiourea, cyanamide, *etc.*, are reported to form coarse low-quality films leading to high dark currents.[133,138] Unlike thermal vaporisation, the direct growth method involves direct contact between the substrate and precursor and its transformation into film over the substrate by thermal polymerisation. Here also, deposition on a variety of substrates like FTO, ITO, *etc.*, is possible. Furthermore, it is feasible to create a variety of morphologies, such as thick films, porous films, or nanorod arrays for g-C_3N_4 films using this method.[139,140] Hetero-films can also be conveniently fabricated *via* vaporization-assisted thermal polymerization. Similarly, choosing special substrates allows the deposition of a continuous film *via* the intermediate formation of a supramolecular complex.[139,141,142] The thin films fabricated using liquid-mediated growth exhibited high mechanical robustness, yielding films that resisted peel-off even after ultrasonication.[142] The microcontact-printing-assisted process involves the infiltration of precursor (cyanamide) solution into the anodic aluminium oxide membrane (AAO) placed between FTO substrates.[143,144] At high temperatures, cyanamide vapours released from AAO diffuse over to the substrates and are deposited as g-C_3N_4 films after thermal polymerisation. The protocol allows the control of film thickness by varying the cyanamide concentration. Solvothermal deposition followed by annealing has also been charted as a convenient route for the fabrication of C_3N_4 films.[144–146] The annealing enables the tri-*s*-triazine structure formation and improves film crystallinity. Altering the precursor concentration, treatment time and post-annealing temperature can control the film thickness and density. The solvothermal route ensures intimate contact between the substrate and the precursors and hence provides better adhesion of the film leading to an enhanced photocurrent.

3. PEC performance of g-C_3N_4 electrodes

The unbiased Fermi level (E_F) position of g-C_3N_4 renders it suitable for application as either the photoanode or the photocathode material for PEC water splitting. The following sections focus on the utility of g-C_3N_4 as photoanodes and photocathodes. The literature reports on photocathodes are relatively few, perhaps due to slow reaction dynamics.

3.1 Pristine and modified graphitic carbon nitride as photoanodes

Although g-C_3N_4 is a promising n-type semiconducting material with appropriate band edge positions, the PEC performance of neat g-C_3N_4 remains low and challenging and efforts have been made to devise strategies for morphological control to obtain a greater photoresponse. The morphological transformation from nanoplates to nanorods *via* controlled reflux resulted in a two-fold enhancement in photocurrent.[147] The alteration from nanoplates to nanorods *via* a sequential exfoliation, regrowth and rolling of lamellar sheets was believed to eliminate the surface defects and increase the active lattice face. DFT studies also supported the stability of the tri-*s*-triazine structure in comparison to the *s*-triazine structure.

Acid exfoliation of bulk g-C_3N_4 could yield a porous honeycomb structure causing a rapid decrease in electron–hole pair recombination.[148] The first successful attempt at microcontact printing-assisted growth over an anodic aluminium oxide (AAO) membrane was reported by Liu *et al.*[144] The random and even diffusion of cyanamide vapours onto the upper and lower substrates resulted in a uniform graphitic carbon nitride network over FTO plates yielding a photocurrent density of 30.2 μA cm^{-2} at 1.23 V_{RHE}. This was ascribed to an advanced microstructure, intimate contact with the conducting substrate, ultrathin film thickness and a high proportion of exposed active sites. Uniform g-C_3N_4 films prepared by thermal vapour condensation from melamine precursors exhibited a high photocurrent density in comparison with bulk g-C_3N_4.[129,133] The high performance was attributed to intimate contact with the substrate, lower charge transfer resistance and reduced electron–hole recombination. The treatment temperature was crucial and relatively smooth transient photocurrents indicated the balanced photo-charge generation and transport process while decay denoted a high probability of charge recombination.

The deposition of FeOOH as a cocatalyst improved the charge transfer rate, giving a high photocurrent.[133]

Zhang *et al.* reported enhanced photocurrent generation in protonated g-C_3N_4 and the protonation was reported to facilitate the dispersion of C_3N_4.[149] An *in situ* solvothermal direct growth of g-C_3N_4 film on an FTO substrate generated a four-fold activity enhancement as compared to post-processed films because of enhanced adhesion and compactness leading to better device performance.[147] Mild annealing in a nitrogen atmosphere was crucial in forming a perfect film. The PEC property of ultrathin flakes of g-C_3N_4 synthesised by a wet mechanical grinding method was reported to be greater as compared to bulk g-C_3N_4 due to two possible reasons: a more positive VB potential and the enhanced electron transfer ability in the horizontal plane prolonging the lifetime of the photogenerated electrons.[150] Pinhole-free g-C_3N_4 films were obtained using a two-step vapour deposition process (TVD) from various precursors, and a photon-induced oxygen evolution upon anodic polarization in aqueous electrolytes resulted in a photocurrent density of 63 μA cm^{-2} at 1.23 V_{RHE} bias.[103] The quality of the films depended on the nature of the substrate, the monomer amount and the deposition temperature. A lower charge transfer resistance at the electrode/electrolyte interface may be ascribed to the enhanced thermal condensation degree of the film prompting the continuous growth of the films. Peng *et al.* fabricated a closely packed g-C_3N_4 film by crystallisation of g-C_3N_4 monomers followed by thermal condensation.[151] The seeded FTO plate was immersed in a hot aqueous supersaturated solution of melamine to prompt further deposition of melamine during cooling followed by calcination to obtain the g-C_3N_4 film. Seeding-induced deposition eventually resulted in the formation of a dense highly interconnected porous layer firmly adhered to the substrate, leading to a low onset potential of 0.25 V_{RHE}. The electrodes also exhibited excellent hole extraction efficiency, promoting exciton dissociation *via* the template confinement along with improved electrode stability. A high IPCE value of around 15% was demonstrated with illumination at 360 nm in a neutral medium without a sacrificial agent.

Monolayered g-C_3N_4 spin-coated onto FTO from a methanolic dispersion of bulk g-C_3N_4 retained its intrinsic n-type properties and activation under positive applied bias-enhanced PEC performance.[102,152] The interaction of the C and N atoms with methanol molecules and the cavitation effects of ultrasonication led to ultrafast drying and disruption of the van der Waals forces within the g-C_3N_4 structure. The negative shifting of the conduction band (CB) and valence band (VB) potentials in exfoliated g-C_3N_4 indicated the possibility of Z-scheme heterojunction construction. Qin *et al.* demonstrated the direct growth of carbon nitride films with extended optical absorption, excellent charge separation under illumination and outstanding performance as the photoanode, yielding 51% faradaic efficiency for O_2 and an external quantum yield of 12% at 1.23 V_{RHE} in alkaline solution and quantum efficiency of around 8.5% at 400 nm without sacrificial agents. In comparison with its bulk counterpart, the nanostructured g-C_3N_4 exhibits a high degree of aromatic ring π-conjugation, enhancing the charge carrier mobility, and the creation of a large proportion of hole-accepting defect sites and space charge regions (SCR) boosts the PEC activity.[153] A high open circuit voltage of 0.61 V indicated the good charge separation characteristics of the electrode. A photoanode based on a vertically aligned g-C_3N_4 porous nanorod array (PNR) prepared *in situ* using a thermal polycondensation approach, with anodic aluminium oxide as the template, could yield a photocurrent density of 120.5 μA cm^{-2} at 1.23 V_{RHE} under solar illumination. The SEM images, transient photocurrent density curves and schematic illustrations showing the transport pathway of electrons in the NPF and PNR of g-C_3N_4 are given in Fig. 4.[154]

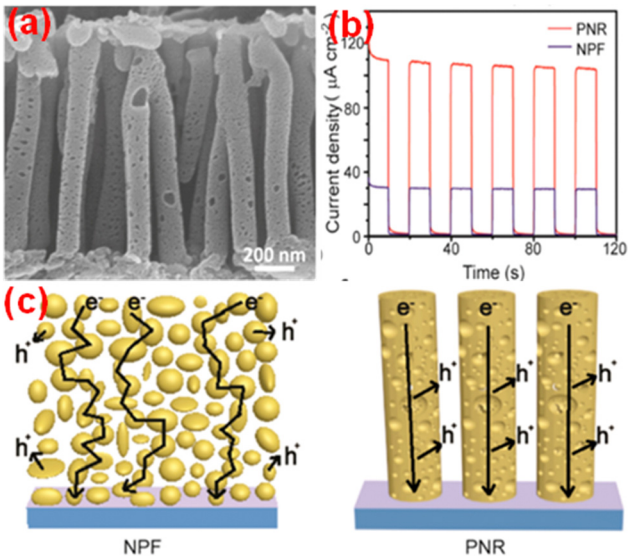

Fig. 4 (a) SEM images, (b) transient photocurrent density curves and (c) schematic diagrams showing the transport pathway of electrons in the NPF and PNR of g-C_3N_4. Reprinted from ref. 154 with permission.

3.1.1 Heteroatom doping. Successful deposition of S-doped g-C_3N_4 films on ITO conductive substrates could be achieved by mixing thiourea into melamine as a co-precursor *via* a CVD route.[140] Apart from introducing sulphur into the matrix, thiourea is proposed to affect the crystallinity and morphology of the films by modulating the polymerisation mode. A negative shift in the open circuit potential indicated the transfer of photogenerated electrons to the counter electrode *via* an external circuit, confirming the n-type behaviour of the electrode. To compensate for the low photocurrent insufficient for O_2 evolution, the feasible construction of n–p heterojunctions as photoanode and n–n heterojunction as photocathode is suggested. The role of S in the initialisation of film growth and in assisting charge migration was proposed by Fang *et al.*[155] A photocurrent of 100 μA cm^{-2} at 1.23 V_{RHE} under AM 1.5 illumination in NaOH electrolyte without a sacrificial agent has been reported. The performance was attributed to the reduced defects along the interface inhibiting charge recombination.[155] Gradient doping of S by molten mediated polymerisation for a gradually varying band structure to promote charge separation and PEC performance in an alkaline

medium was demonstrated by Fang *et al.*[156] P and S-doped 1D-g-C_3N_4 prepared using a modified hydrothermal synthesis exhibited high water oxidation capability.[157] Enhanced charge separation and subsequent prolonging of the lifetime of charge carriers resulted in the charge accumulation at the electrode surface and transfer to the electrolyte yielding a higher water photo-oxidation current as compared to undoped 3D and 1D-g-C_3N_4. The promotion of PEC activity by the synergistic effect of heteroatom doping/heterojunction formation/cocatalyst deposition on interfacial charge transfer has also been demonstrated.[158–165]

A drastic narrowing of the bandgap in P-doped g-C_3N_4 enabled near-infrared light-induced PEC water splitting, generating a photocurrent density of 1.4 μA cm^{-2} at 1.2 $V_{Ag/AgCl}$ and H_2 evolution of 1.27 μmol h^{-1} g^{-1} at 0.6 V with reference to the Ag/AgCl electrode.[166] The delocalisation of the isolated electrons into the π-conjugated structure of g-C_3N_4, generated a positively charged centre at the P atom inhibiting the charge recombination. A novel B-C_3N_4/bulk g-C_3N_4 heterojunction architecture with 10% IPCE and 103.2 μA cm^{-2} at 1.23 V_{RHE} was reported by Ruan *et al.*[137] Theoretical and experimental investigations indicated an upward shifting of the VB edge and a lowering of the bandgap enabling the hole transfer from the bulk to the surface for photooxidation/hydrogen evolution and enhanced PEC activity.[72,137] The results of PEC measurements from ref. 72 are represented in Fig. 5. A high level of boron doping induced the formation of defect centres promoting electron–hole recombination. The negligible impact of H_2O_2 addition on the photocurrent proves the inherent charge separation in the photoanode. The localisation of HOMO (VB) onto two heptazines and the delocalisation of LUMO (CB) was proposed by the theoretical studies indicating the possible pathway of suppression of electron–hole recombination. Lei *et al.* constructed a g-C_3N_4/B-doped g-C_3N_4 (BCN) 2D heterojunction photoanode, which intensified the interfacial contact area between BCN and the porous g-C_3N_4 and shortened the transfer time and diffusion pathlength of photogenerated charge carriers.[161] A heat treatment strategy was used for the preparation of B-doped graphitic carbon dots/C rich g-C_3N_4 heterojunction composites with higher photocatalytic and photoelectrochemical activity.[162]

V-doped g-C_3N_4 prepared by the direct calcination of urea and ammonium metavanadate exhibited enhanced light absorption and charge separation, and high water-splitting activity.[167] Doping with cobalt resulted in the VB being shifted to more positive values and a negative shift of the CB edge, improving the PEC performance.[84,168] The red shift in the absorption edge enhanced the light-harvesting capability, and improved interfacial charge transfer was established from the EIS analysis, with Co^{2+} acting as an electron trap. The role of Co in promoting O_2 evolution was also reported.[168] Pd and Ag-doped C_3N_4 nanostructures electrophoretically deposited on FTO for photoelectrocatalytic oxygen evolution under simulated solar radiation have been tested.[169] Dip coating of $Ni(OH)_2$ further improved the performance. An increased band bending at the band edge and facilitated electron transfer at the electrode/electrolyte interface enhanced the surface oxidation kinetics. Zhao *et al.* devised an ionic liquid-assisted protocol for the synthesis of Br-modified g-C_3N_4 with high surface area and porous structure.[170] The enhanced transportation capability of photogenerated electrons and improved optical/conductive properties are attributes of high H_2 evolution capability. Significant enhancement in the photoelectrochemical properties was achieved by the insertion of Ni ions into the phenyl-modified graphitic carbon nitride layer.[75] Interactions between Ni and precursor molecules in the molten state, prior to condensation, contributed to the homogeneous dispersion of Ni, leading to extended light absorption and charge transfer, culminating in enhanced PEC performance. The reduction in the bandgap after bismuth doping is linked to the formation of localized isolated energy levels below the CB minima of pristine C_3N_4.[102] Bi-doping of g-C_3N_4 significantly favors the charge separation and electron transfer from the surface of the photoanode to the electrolyte, with the PEC performance being strongly dependent on optimal Bi content. To enrich the photoactivity, Paul *et al.* adopted the co-doping of Mg and Li atoms into the g-C_3N_4 matrix, resulting in a greater photo response as compared to its metallic counterparts.[171]

3.1.2 Carbon materials. Carbon materials can act as excellent matrices facilitating electron transfer to enhance PEC performance. Carbon nanomaterial insertion is proposed to provide orthogonalization of light resulting in enhanced light absorption.[172] The PEC performance of g-C_3N_4 was improved through the efficient charge cascade achieved by Bi doping along with the use of GO as a cocatalyst on the surface of the photoanode.[165] A low Tafel slope and better interfacial charge transfer prospects revealed by EIS and PL analysis account for better electrode kinetics and reduced activation energy barrier for the OER. The development of a highly porous interconnected g-C_3N_4/r-GO photoanode with long electron diffusion length (≈36 μm), large electrochemically active surface area, enhanced light harvesting, and hole extraction property was reported by Peng *et al.*[116] Better interfacial charge transfer and excellent electron mobility led to a 20-fold enhancement in photocurrent density, a high external quantum efficiency of ≈5% at 400 nm and stability over a wide pH range. A porous graphitic carbon nitride/reduced graphene oxide (r-GO) interface constructed *via* a solvothermal route and deposited on a Ni foam created a highly active photoanode, with r-GO acting as the bridge for accelerating the rate of electron transfer from

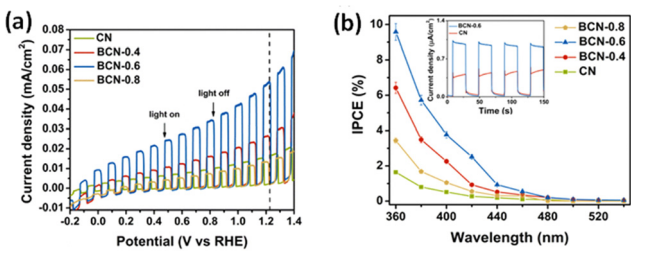

Fig. 5 (a) The light-chopped LSV curves in 0.2 M Na_2SO_4 and 0.05 M Na_2S (pH = 11.7). (b) The IPCE with transient photocurrent density curves under visible light (λ > 420 nm) (inset). Reprinted from ref. 72 with permission.

g-C_3N_4 to Ni foam.[173] The efficient transfer of the hot electrons generated from g-C_3N_4 under visible light illumination to the cathode was efficiently driven by r-GO and external bias potential. g-C_3N_4/CNT composite films with enhanced PEC properties were fabricated by Yousefzadeh *et al.*[174] The mechanism proposed involves water oxidation by the holes. CNT promotes the transport of the photoelectrons from the g-C_3N_4 nanoparticles to the counter Pt electrode *via* the FTO substrate, leading to water reduction. A metal-free flexible protonated g-C_3N_4/C dots photoanode fabricated on a polyethylene terephthalate (PET)/indium tin oxide substrate (ITO) by the electrophoretic approach generated a photocurrent of 38 μA cm^{-2} at 1 V_{RHE}.[175] The narrow band gap sp^2 carbon clusters contributed to excellent light absorption and a negative shift in the onset potential.

3.1.3 Metal oxides. TiO_2 has been one of the most explored wide-bandgap materials. Heterojunction formation with g-C_3N_4 along with enhancing the visible light sensitivity improves charge separation and enhances the PEC performance.[176] As compared to TiO_2 nanocrystal-based films, unique nanotube arrays are found to exhibit higher photon collection efficiency and better charge separation.[177,178] g-C_3N_4 and TiO_2 nanotube arrays with 7.3% IPCE at a wavelength of 400 nm were fabricated by Zhou *et al.*[179] Direct Ti–O–C bonding resulted in unique electronic coupling and enhanced optical absorption.[134] Electron injection from the LUMO of g-C_3N_4 to the CB of TiO_2 offers efficient charge separation and the coupled system can be regarded as a "dyad". A photoanode comprised of g-C_3N_4–TiO_2 nanotube arrays with UV and near-UV sensitivity was fabricated by the *in situ* growth of g-C_3N_4 on the surface of TiO_2 nanotubes, resulting in a six-fold enhancement in photocurrent density and hydrogen evolution of 19.1 μmol h^{-1}.[180] Cu implantation enhanced the electronic conductivity and electronic structure of TiO_2 nanotube arrays (TNA), causing a significant lowering of the band gap, and further decoration with polymeric carbon nitride nanosheets (PCN) enhanced visible light absorption and exciton separation at the heterojunction. Cu implantation generates Ti^{3+} in TiO_2 crystals and enhances interfacial bonding between TiO_2 and PCN with a subsequent acceleration of charge transfer at the heterojunction. PCN decoration passivates the surface defects created by Cu implantation and reduces the surface trap density of the material enhancing exciton lifetime.[181] Synthesis of TNAs by electrochemical anodization on a titanium substrate and the facile thermal treatment using suitable substrates for the formation of g-C_3N_4/TiO_2 heterojunction is one of the most adopted strategies.[182–184] A diagram of the charge transfer mechanism of the g-C_3N_4/TNTA heterojunction electrode and the photocurrent density of different photoanodes is given in Fig. 6.[184] The interaction involves the charge transfer from the electron-rich C_3N_4 surface and the unoccupied orbital of Ti^{4+}. The synergistic effects of Ti^{3+} and O-doping on the photoelectrochemical performance of Ti^{3+} self-doped TiO_2/oxygen-doped g-C_3N_4 (Ti^{3+}–TiO_2/O–g-C_3N_4) heterojunctions were examined.[103] C–O and O−C−N bonds in O–C_3N_4 can be bonded with hydroxyl groups of TiO_2 to form electron transfer pathways.

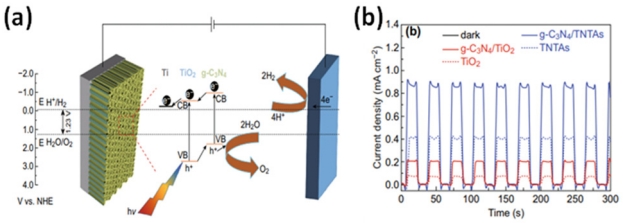

Fig. 6 (a) A schematic depiction of the charge transfer mechanism of the g-C_3N_4/TNTA heterojunction electrode. (b) Time-dependent photocurrent density under intermittent light irradiation. Reprinted from ref. 184 with permission.

A core–shell TiO_2/g-C_3N_4 structure, obtained by the hydrothermal growth of TiO_2 nanorods and solvothermal growth of the g-C_3N_4 layer, was investigated by Fan *et al.*[185] g-C_3N_4 acts as a visible light absorption layer, while TiO_2 acts as an effective electron transfer layer hindering electron–hole recombination and improving the overall performance.[186] The construction of a Z-scheme heterostructure of TiO_2 with an interfacial oxygen vacancy layer and coupling with g-C_3N_4 has been investigated.[187,188] The oxygen vacancies triggered the onset of an electronic band below the CB of pure TiO_2. High donor density and a more negative flat band potential imply better photoelectrochemical performance. The enhanced photoelectrochemical performance of TiO_2 nanorod arrays/pillars decorated with g-C_3N_4 quantum dots has been verified by several groups.[189–191] The synergistic effects of TiO_2 and C_3N_4 were established by DFT calculations.[189] Exposure to barbituric acid and the subsequent thermal polymerisation led to the substitution of N with C, producing reactive N-defect sites with an ensuing enhancement in PEC hydrogen evolution and exceptional stability for around 111 h under continuous illumination.[191] Ultrathin red 2D-g-C_3N_4 (red CN) with a band gap of 2.05 eV enabling strong band-to-band visible light absorption was realised by the fluorination of ultrathin g-C_3N_4 followed by thermal defluorination.[192] An intermediate defect band led to a lowering of the CB and the associated distribution of defect centres imparted high light-harvesting power and suppressed the recombination rate. A TiO_2 nanorod-based photoanode sensitized by red 2D CNs formed a type II band alignment showing a superior photocurrent density of 121.9 μA cm^{-2} at 1.23 V_{RHE} without the aid of a co-catalyst. A type II heterostructure between g-C_3N_4 nanoplatelets and TiO_2 giving a photocurrent density of 142.7 μA cm^{-2} at 1.23 V_{RHE} was reported by Rajaitha *et al.*[193] A photoanode with a shell-core heterostructure of N-doped C/g-C_3N_4/TiO_2 generating a photocurrent density of 0.45 mA cm^{-2} at 0.6 V was constructed by Huang *et al.*[194]

Improvement in electrical conductivity *via* reinforced contact between TiO_2 and g-C_3N_4 could be accomplished in a nitrogen-doped carbon (C_N) interfacial nano-layer derived from polydopamine. g-C_3N_4-wrapped TiO_2 NTA heterojunction photoelectrodes with effective interfacial charge separation were fabricated *via* a chemical vapour deposition-like process.[195] Niobium doping has been a good strategy for altering the electronic

properties of TiO_2 due to the size compatibility of Nb^{5+} and Ti^{4+}. Nb^{5+} replaces Ti^{4+} and the donor is formed on the TiO_2 conduction band, providing electrons for Ti^{4+} and obtaining high carrier concentration, enhancing the conductivity, and improving the PEC performance of the Nb–TiO_2/g-C_3N_4 photoanode.[196] The successful formation of a P–C_3N_4/TiO_2 heterojunction *via* sequential electrochemical anodization, wet dip coating and thermal polymerisation, and its efficient photocatalytic and photoelectrocatalytic performance has been demonstrated.[159] TiO_2 nanorods decorated with B-doped g-C_3N_4 were fabricated *via* the thermal polymerisation method to improve the PEC performance. The rational design of a hydrophilic bifunctional hierarchical assembly of B-doped g-C_3N_4 nanoplatelets with high visible light sensitivity and suppressed charge recombination was attempted by Ding *et al.*[197] The synergistic effect of B doping and the hydrophilic character, coupled with increased specific surface area and improved hierarchical porosity generated a photocurrent density of 1.72 mA cm^{-2} at 1.23 V_{RHE} under AM 1.5G illumination. The modulation of the electronic structure was proposed to be *via* an orbital overlap between 2p levels of B and C in the VB and that of N and B in the CB. The synthesis of fluorine-doped g-C_3N_4 QDs (CNFQD) *via* a solid-state reaction and its further embedding into rutile TiO_2 by an *in situ* hydrothermal process could extend the photo response to 500 nm.[198] The energetics at the heterojunction were favourable for efficient electron transfer from CNFQDs to TiO_2 and hole transfer to the electrolyte under visible light irradiation. Modification of g-C_3N_4/TiO_2 with Co–Pi is reported to be a competent strategy for augmenting charge migration.[199,200] Co–Pi incorporation does not change the band positions and the band gap was evidenced by the almost similar flat band potentials of g-C_3N_4/TiO_2 and Co–Pi-modified g-C_3N_4/TiO_2. The high PEC performance could be attributed to the fast interfacial charge migration from the photoanode to the electrolyte mediated by Co–Pi. The protective function of the TiO_2 layer and hole capture layer is also well demonstrated.[200]

Cobalt atoms when coordinated with g-C_3N_4 are reported to act as co-catalysts for water oxidation, leading to a photocurrent of 1.79 mA cm^{-2} at 1.23 V_{RHE}.[201] The coordination was confirmed by the blue shift in the distinctive bending vibration of the tri-*s*-triazine unit ascribed to the weakening of the conjugation effect due to electron transfer from the π-conjugated ring to the empty d orbital of Co^{2+}. The conversion of Co^{II} to Co^{III} and Co^{IV} mediated by photogenerated holes reduces the kinetic barrier for water oxidation and improves the water-splitting performance. The excellent PEC activity of the CuNi@g-C_3N_4/TiO_2 system was ascribed to the cooperative effects induced by the creation of a heterojunction between TiO_2 and g-C_3N_4 photocatalysts and a subsequent enhancement in optical absorption and charge separation evoked by Cu species and the co-catalytic effect of $Ni(OH)_2$ toward the oxygen evolution reaction.[202] A ternary photoanode of carbon dots (CD)/ultrathin carbon nitride (UCN) coupled to TiO_2 nanorods with improved PEC activity was fabricated by Kong *et al.*[203] While CDs can significantly facilitate the decomposition of H_2O_2, an intermediate of two-electron water oxidation, and induce rapid reaction kinetics, UCN efficiently accelerates charge separation and restricts electron/hole recombination. The TiO_2/g-C_3N_4/CNT photoanode with excellent stability and an onset potential of 0.25 $V_{Ag/AgCl}$ has been reported.[204] The excellent photochemical performance benefits from the migration of photoinduced electrons from g-C_3N_4 to TiO_2 and their intimate interface contact with CNT. A hierarchical Co_3O_4/P–C_3N_4/TiO_2 photoanode with matched and continuous energy band positions was designed for visible-light-driven PEC water splitting.[205] Swift diffusion of the photogenerated holes from the 1-D TiO_2@P–C_3N_4 core–shell structure to the surface of the 0-D Co_3O_4 nanodots and consecutive transfer of the photogenerated electrons to the counter electrode contributes to the high PEC performance. The short diffusion path for holes through highly dispersed 0-D Co_3O_4 nanodots inhibits the accumulation of holes.

A morphology-controlled synthesis of g-C_3N_4/Fe_2O_3 composites resulted in enhanced interfacial charge transfer.[206] Small amounts of α-Fe_2O_3 nanosheets are reported to promote the exfoliation of g-C_3N_4, producing a 2D hybrid that exhibits tight interfaces forming a Z-scheme junction.[207] Ti^{4+} doping of Fe_2O_3 promoted the charge transfer due to enhancement in the conductivity of bulk Fe_2O_3.[104] The electrostatic self-assembly of negatively charged Fe_2O_3 and protonated C_3N_4 forming a Z scheme with hydrogen bond-facilitated charge transfer has been reported.[96] Aerosol-assisted chemical vapour deposition (AACVD) and the ensuing spin coating and air annealing have been employed for the creation of α-Fe_2O_3/g-C_3N_4 heterojunction photoanode.[167] The unique nanoflake structure of α-Fe_2O_3 promotes good adhesion with g-C_3N_4, leading to strong interfacial contact and lends admirable stability to the photoanode. The intimate contact at the heterojunction facilitates the electron transfer from the CB of g-C_3N_4 towards the less negative CB of α-Fe_2O_3 and hole transfer from the more positive VB of α-Fe_2O_3 to that of g-C_3N_4. The consequent accumulation of electrons in α-Fe_2O_3 and holes in g-C_3N_4 prevents the charge recombination and eventually leads to enhanced PEC performance.[208] Integration of the Co–Pi cocatalyst promoted water oxidation, yielding a high photocurrent density.[209,210] The synthesis of narrow band gap wine-red carbon nitride (WRCN) from carbon-rich supramolecular precursors and the subsequent coupling with Fe_2O_3 forming a type II heterojunction have been attempted.[210] WRCN showed enhanced absorption extending to the near IR region, probably due to a high degree of polymerisation facilitated by molten salts like NaCl/KCl used in the ionothermal method. High PEC activity of metallic and bimetallic carbon nitride integrated with hematite was reported.[211,212] The surface modification of a hematite dendrite/g-C_3N_4 composite with an oxidation cocatalyst ($CoFeO_x$) could achieve enhanced visible-light-induced PEC water splitting.[211] The higher electronic conductivity of the $CoFeO_x$ layer enables effective charge transfer at the electrode/electrolyte interface during water oxidation. The breakage of electroneutrality and the formation of a tubular structure, depending on the annealing temperature, have been postulated.[212] The bending of carbon nitride sheets to the tubular structure with

cobalt embedded in the center was proposed to be aided by the Co site. An integrated photoanode constructed with carbon quantum dot (CQD)-sensitized Ti:Fe_2O_3@graphitic carbon nitride nanosheets (GCNNS) core–shell array displayed a photocurrent density of 3.38 mA cm^{-2} at 1.23 V_{RHE}.[213] Ti^{3+} effectively boosts bulk charge separation, as revealed by the anodic shifting of the flat band potential, while CQDs aid in charge carrier separation and a shift in the onset potential of the photoelectrode due to its inherent capability of H_2O_2 oxidation. Interfacial coordination between C_3N_4 and CdS–Fe_3O_4 promoted the band gap-dependent interfacial charge transfer and contributed to the overall PEC performance of the ternary system.[214] N-doped carbon dots were anchored on g-C_3N_4/Fe_2O_3 for the degradation of trimethoprim and H_2 evolution from wastewater.[215]

Absorption in the visible region, good electron transport properties, photocorrosion resistance, chemical/thermal stability, and band edges suitable for water splitting render WO_3 a promising material for energy harvesting. g-C_3N_4/WO_3 heterojunction plate array films were synthesised through combinative hydrothermal and dipping-annealing methods.[216] As-prepared g-C_3N_4/WO_3 heterojunction films achieved a maximum photocurrent density of 2.10 mA cm^{-2} at 2 V_{RHE}, almost 3-fold higher than pure WO_3 film. In the heterojunction film, the photo-generated electrons of g-C_3N_4 easily migrate to the CB of WO_3 and then to the FTO substrate and reach the counter electrode through the external circuit. Similarly, the photogenerated holes of WO_3 transferred to the VB of g-C_3N_4 can take part in the oxygen evolution reaction.[216–218] The substantial stability of WO_3/g-C_3N_4 nanosheet photoanodes after continuous illumination for 3600 seconds, and efficiency for seawater splitting have also been reported.[217] The order of the deposition clearly influenced the type of heterojunction formed and significantly affected the PEC performance.[81] The Z-scheme g-C_3N_4/NCDs/WO_x photocatalyst, where nitrogen-doped carbon dots (NCDs) acted as the electron mediator, exhibited an apparent quantum efficiency of 7.58% at 420 nm.[97] The localised surface plasmon resonance effect of WO_x and the photoluminescence property of NCDs enhanced the NIR utilisation efficiency. Nanobelt-like WO_x overlapped with NCDs on the surface of CN nanosheets and the close solid−solid interface ensured the fast charge mobility.

ZnO/C_3N_4 type II heterojunctions have been explored for their photoelectrochemical performance.[219–223] The surface deposition of g-C_3N_4 on ZnO nanowires/nanorods with smooth and rapid interfacial electron transfer has been attempted. The incorporation of Pt clusters formed a ternary photoanode generating a photocurrent density of 120 μA cm^{-2} at 0.5 $V_{Ag/AgCl}$ in a 0.5 M Na_2SO_4 solution.[219] Both g-C_3N_4 and ZnO acted as light absorbers while Pt nanoclusters served as the cocatalyst facilitating the transfer of the photogenerated electrons. Sulphuration of the ZnO electrode could form core–shell ZnO/ZnS heterostructures, which were further integrated with C_3N_4 to obtain ternary photoanodes with enhanced PEC performance.[221] The sulphurisation process occurs *via* anion exchange through which surface trap states such as oxygen vacancies and adsorbed oxygen of pristine ZnO nanorods become further reduced to form the ZnS interlayer. Type II photoanodes were designed by coating PCN films onto highly conductive yttrium (Y)-doped zinc oxide (ZnO) nanorods (NRs) serving as charge collectors.[100] Bifunctional CoPi efficiently inhibited the photocorrosion of g-C_3N_4/ZnO and provided a hole transfer channel.[224] Further, the Fermi level potential of g-C_3N_4@ZnO shifted towards the positive direction with a resultant upward band-bending at the band edge position, promoting the separation efficiency of the photogenerated electron–hole pairs.[225] CdS quantum dots modified g-C_3N_4/ZnO nanorods core–shell structures were fabricated *via* hydrothermal and SILAR (successive ionic layer adsorption and desorption) processes. The photogenerated electrons in g-C_3N_4 and CdS were transported to ZnO and the Pt electrode for the HER.[226] Masoumi *et al.* constructed a dual heterojunction of ZnO with Fe_2O_3 and g-C_3N_4, which facilitated electron–hole separation to the surface of the substrate, thereby increasing the PEC performance.[227]

SnO_2 is one of the most investigated wide band gap materials for energy-harvesting applications. SnO_{2-x}/g-C_3N_4 heterojunction nanocomposites were prepared by a convenient one-step pyrolysis method.[103] Ultrasonication ensures the homogenisation of $Sn(OH)_4$ with melamine due to the formation of hydrogen bonds; during the thermal treatment, melamine decomposes into g-C_3N_4, releasing reducing gases such as NH_3, with the consequent formation of SnO_{2-x}. This has been reported to enhance charge-carrier mobility, and visible-light absorption capability is achieved due to the presence of oxygen vacancies in nonstoichiometric (reduced) semiconductor nanocrystals. The homogeneous deposition of g-C_3N_4 nanodots in amorphous mesoporous 1D SnO_2 as the host *via* pulsed electrophoresis followed by water soaking treatment to crystallize amorphous SnO_2 could yield extended visible light absorption and deliver a photocurrent density of 1.8 mA cm^{-2} at 0.2 $V_{Ag/AgCl}$.[228] Incorporating plasmonic Au into the SnO_2 quantum dots (SQD) improved the performance by providing a pathway for the transportation of electrons from g-C_3N_4 to SQD.[229] The band-bending strategy effectively separates the electron–hole pair, thereby improving the PEC performance.

p-type NiO exhibits strong resistance to photo-corrosion in neutral electrolyte solutions. It shows perfect lattice matching with g-C_3N_4 and possesses a compatible band alignment, enabling the formation of a type II heterojunction. The more positive VB potential of NiO enables the injection of photogenerated holes from g-C_3N_4 to NiO, suppressing the charge-recombination by effectively passivating the surface-trapped electrons. A 2D/2D interface between Ni/NiO hexagonal nanosheets and g-C_3N_4 *via in situ* solid-state heat treatment exhibited superior activity for electrochemical and photoelectrochemical water splitting.[230] The use of a liquid-phase laser ablation technique for the heterostructured nanocomposite NiO@g-C_3N_4 has been reported.[231]

3.1.4 Tungstates and vanadates. Bi_2WO_6 QDs coupled with g-C_3N_4 form a Z scheme and the one-step hydrothermal synthesis mediated by oleate ions prevented the aggregation of Bi_2WO_6 QDs.[232] A type II heterojunction of S-doped g-C_3N_4/Bi_3WO_6 was fabricated from an ultrasonication approach to

overcome the sluggish charge transfer at the electrode/electrolyte interface and fast recombination of electron–hole pairs of Bi_2WO_6 (BWO).[233] It has been speculated that in S-doped g-C_3N_4 (SCN), the VBM is located on N atoms except for the N atom near sulfur, while CBM is mainly located on the S atom at the adjacent heptazine unit. This enhances the photogenerated electron–hole pair separation, reducing recombination and enhancing the photocatalytic efficiency.[234] The electron migration process generates the positively charged electron depletion layer in SCN near the interface, which leads to the upward bending of the band edge. Similarly, an electron accumulation layer in the BWO near the interface causes the downward bending of the band edge in BWO. The resultant inner electric field (IEF) at the interface resists further electron transfer. The energy level positioning favours the formation of a type II heterojunction with facile electron transfer. A 2D/1D heterostructure with $ZnWO_4$ nanorods decorated over the g-C_3N_4 nanosheets (g-C_3N_4/$ZnWO_4$) was successfully fabricated by hydrothermal synthesis.[235] The band gap modification was attributed to the band bending arising due to heterojunction formation.

$BiVO_4$ has been well explored as a photocatalyst and photoelectrocatalyst due to its visible light sensitivity, band edge positions suitable for hydrogen evolution and high stability. A Z-scheme mechanism at the g-C_3N_4/$BiVO_4$ interface has been well established.[236,237] The relative band positions induce the injection of excited electrons on the CB of $BiVO_4$ into the VB of g-C_3N_4 to recombine with photogenerated holes and restrain recombination. The CB of g-C_3N_4 and the VB of $BiVO_4$ were projected as the centres for reduction and oxidation, respectively. Uniform films with good coverage and crack-free surfaces could be obtained by electrospinning and the nanostructured heterojunction facilitated the electron–hole separation due to a shorter charge transport distance with a consequent high photocurrent density and negative shift of onset potential.[114] The augmented activity of g-C_3N_4/$BiVO_4$ microflower structures has been reported.[238] g-C_3N_4 nanolayers self-assembled with $BiVO_4$ into a highly coupled g-C_3N_4/$BiVO_4$ dyad augmented the charge separation efficiency of the $BiVO_4$ photoelectrodes for the OER.[239] The incident photon-to-current conversion efficiency (IPCE) provided by the scalable g-C_3N_4/$BiVO_4$ photoanodes was estimated to be 50% at 1.23 V_{RHE} in 0.5 M Na_2SO_4 solution and significantly increased to 97% at an applied voltage of 1.6 V_{RHE}. The enhanced visible light absorption of the dyads was attributed to the multiple reflections of light rays in the hierarchical structure attained by the introduction of g-C_3N_4 nanolayers. The g-C_3N_4 nanolayers function as the pump to extract electrons from the $BiVO_4$ side for better OER performance, with the pumping effect being enhanced by the bias voltage. Ultrathin g-C_3N_4 nanosheets were projected as an efficient metal-free cocatalyst for improving the oxygen evolution activity of the nanoporous $BiVO_4$ photoanode.[240,241] Fig. 7 represents the illustration of the exfoliation/acidification process for fabricating $BiVO_4$/g-C_3N_4-NS photoanodes with enhanced PEC performance. The g-C_3N_4 nanolayers not only suppress the surface charge recombination of $BiVO_4$ but also effectively accommodate

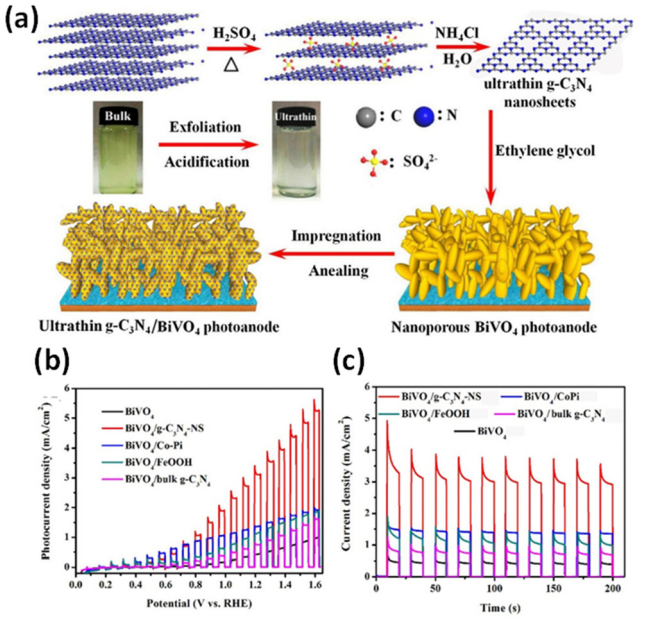

Fig. 7 (a) Schematic illustration of the exfoliation and acidification process for the fabrication of $BiVO_4$/g-C_3N_4-NS photoanodes. Reprinted from ref. 240 with permission. (b) *J*–*V* curves, (c) transient photocurrent response (1.23 V *vs.* RHE) for different photoanodes measured under visible-light illumination in 0.1 M Na_2SO_4. Reprinted from ref. 242 with permission.

photogenerated holes in the VB for water oxidation. Mo doping of $BiVO_4$ enhances the charge separation due to exceptional electron transfer capability.[239,240] Mo doping significantly reduces the interfacial energy loss *via* work function adjustment and increases the open circuit photovoltage of $BiVO_4$.[242] A similar effect is generated at the B-C_3N_4 interface rendering an IPCE of 2.67% at 0.54 V_{RHE} for the B-C_3N_4/Mo–$BiVO_4$ heterojunction. The inclusion of $NiFeO_x$ as an oxygen evolution catalyst greatly improves the PEC performance. The DFT simulations proposed the separation of electron/hole pairs facilitated by the creation of an internal electric field at the g-C_3N_4/$BiVO_4$ interface *via* the formation of a van der Waals-type heterojunction.[105] A combined theoretical/experimental approach was adopted by Mohamed *et al.* to establish the boosted performance of the γ-irradiated g-C_3N_4/$BiVO_4$ heterojunction.[243] γ irradiation was observed to alter the surface topology and the enhancement in optical properties was attributed to the hybridisation of C 1s and N 1s. A combined theoretical and experimental study was conducted on the g-C_3N_4/$BiVO_4$ heterojunction synthesised by a modified sol–gel technique by varying the weight ratios of g-C_3N_4.[244] A comparative evaluation of the impact of carbon nanotubes, reduced graphene oxide and graphitic carbon nitride in enhancing the PEC performance of $BiVO_4$ has been attempted and the maximum IPCE was reported for the g-C_3N_4/$BiVO_4$ heterojunction.[245] The band bending at the nano junction was estimated to reduce bulk recombination and facilitate charge transport and transfer. The boosted PEC performance could be correlated to efficient charge transfer kinetics as a result of the increased number of charge carriers and the lowering of the

charge transfer resistance. Samsudin *et al.* reported the augmented photoelectrocatalytic performance of the g-C_3N_4/$BiVO_4$ microflower composites with supporting theoretical studies.[238] The photocatalytic and photoelectrochemical performances of g-C_3N_4/$InVO_4$[246] and $FeVO_4$/g-C_3N_4[247] systems have also been reported.

3.1.5 Chalcogenides. The outstanding mechanical and electrical properties of molybdenum disulfide (MoS_2) with a 2D layered structure attracted much attention and it has been extensively explored as a hydrogen evolution catalyst.[248] Metallic MoS_2 loaded on g-C_3N_4 showed an enhancement in PEC performance and photochemical H_2O_2 generation.[249] The layered MoS_2 co-catalysts were distributed on the surface of g-C_3N_4 *via* a facile impregnation method and the formation of intimate interfaces facilitated charge transfer and visible light sensitivity.[250] The interfacial transfer of photogenerated electrons in the CB of g-C_3N_4 to MoS_2 renders the conduction band electrons more mobile, enabling the separation of electron–hole pairs. The hydrothermal growth of MoS_2 over the S-doped g-C_3N_4 deposited *via* CVD on the ITO substrate formed a p–n junction with high PEC performance due to the synergistic effect arising from high charge carrier concentration, efficient charge separation and enhanced light absorption.[251] Ye *et al.* reported an n–n type heterojunction with a typical type II band structure.[252]

Plasmonic Bi nanoparticles supported over a g-C_3N_4/Bi_2S_3 photoanode for PEC water splitting were reported by Subramanyam *et al.*[253] Decoration of Bi_2S_3 QDs on g-C_3N_4 extended the absorption edge to the near-infrared region and it was further enhanced by the plasmonic effect of Bi nanoparticles. The maximum photocurrent at around 310 nm could be attributed to the formation of energetic hot electrons, and the presence of Bi nanoparticles accelerated the overall charge transportation, resulting in PEC-driven hydrogen generation. The intimate In_2S_3/g-C_3N_4 interface promoted charge transfer and inhibited the recombination of electron–hole pairs, significantly improving the PEC performance.[254,255] The highly conductive In_2S_3 rapidly withdraws electrons from g-C_3N_4, transferring them to ITO. Meanwhile, the photogenerated holes in the g-C_3N_4 nanosheets are transferred to In_2S_3 NPs and are consumed at the In_2S_3/g-C_3N_4-electrolyte junction. The PEC activity and stability were greatly enhanced by combining CdS and g-C_3N_4 through the formation of an interlocking thin film, which provided a large contact area and better adhesion to FTO.[256] Due to the higher positioning of the VB and CB of C_3N_4 relative to CdS, the photoexcited electrons of g-C_3N_4 were directly transferred to CdS, and the holes in the valence band of CdS migrated to the conduction band of g-C_3N_4. The Ag@g-C_3N_4/ZnS photoanode with a photocurrent turn-on potential of 0.45 V_{RHE} has been reported.[257] The light passed through the transparent Zns layer to Ag@g-C_3N_4 and then to TiO_2, an electron-selective layer, which enhanced the transfer of electrons to the circuit while the incorporation of $Ni(OH)_2$ improved the stability of the photoanode and its water oxidation capability. Chaudhary *et al.* reported the synthesis of copper sulphide (CuS) supported on Ni-incorporated graphitic carbon nitride sheets. The improved activity was assigned to the band bending induced by the larger space region width, the formation of an effective p–n junction between CuS and g-C_3N_4 lowering the effective band gap, and the facile charge transfer kinetics due to Ni incorporation into the g-C_3N_4 matrix.[164] The conceptual design of the InSe/g-C_3N_4 van der Waals heterostructure with type II band alignment to achieve spontaneous and highly efficient water splitting was proposed by He *et al.*[258]

3.1.6 Layered double hydroxides (LDH). The special interest in layered double hydroxides (LDH) in catalysis can be traced to their lamellar structure, redox properties, non-toxicity, and high structural stability. The formation of oxo-bridges facilitates the metal-to-metal charge transfer, thereby decelerating the electron–hole recombination.[259,260] The *in situ* assembly of N-deficient porous carbon nitride nanosheets and the NiFe-layered double hydroxide into a 3D N-doped graphene framework was attempted by Hou *et al.* to obtain a 3D hierarchical nanostructure.[261] The ternary hybrid exhibited remarkable photoelectrochemical performance for water oxidation, which was attributed to the effectual light trapping, multidimensional electron transport trails, rapid charge transport, strong coupling effect and amended surface reaction kinetics. CoMn-LDH[262] and CoFe-LDH[263] coupled with g-C_3N_4 for high photoelectrochemical performance have been reported.[262] NiCo-LDH was introduced onto g-C_3N_4 film through cathodic electrochemical deposition and acted as a co-catalyst for water oxidation.[264] N-doped graphene, introduced into the heterostructure assembly of the g-C_3N_4/NiFe LDH hybrid behaves as an electronic mediator to strengthen the interfacial interactions and charge transfer.[265] A Z-scheme charge transfer mechanism due to enriched oxygen vacancy defects in NiFe-LDH and N-r-GO contributes to the superior photoactivity of the heterostructure. The ruptured tubular structure of graphitic carbon nitride (RT g-C_3N_4) was reported to improve charge separation.[85] Efficient photoelectrochemical water oxidation proceeded over the CuTi-LDH/g-C_3N_4 type II heterojunction.[266] Bismuth oxycarbonate ($Bi_2O_2CO_3$) grafted NiFe LDH on g-C_3N_4. Interfacial electron transfer aiding photoelectrochemical water splitting *via* the S-scheme mechanism has also been demonstrated.[267]

3.1.7 Miscellaneous. Samanta *et al.* reported the plasmonic enhancement of H_2 evolution over Au/C_3N_4 systems.[121] The induced plasmonic resonance of Au NPs augmented the electron passage through the Schottky barrier at the Au/g-C_3N_4 interfaces and the accumulation of many electrons in the CB leads to high photocurrent and H_2 evolution. A hierarchical core–shell copper–azolate-C_3N_4 framework (CuAF) integrated with $Ni(OH)_2$ as the cocatalyst forming a staggered-gap type II heterojunction for water oxidation was constructed by Karimi-Nazazbad *et al.*[268] The relative positioning of the valence and conduction bands in the heterojunction resulted in the accumulation of electrons and holes in the CB of C_3N_4 and valence band of CuAF, respectively. The construction of a photoanode by loading 2D crystallised $Ni(OH)_2$ on the surface of three-dimensionally microporous g-C_3N_4 *via* an electrostatic method was demonstrated by Cao *et al.*[269] The resultant Z scheme heterojunction accelerated the charge carrier separation while the 2D/3D hollow structure facilitated their diffusion.

Bismuth oxyhalides are characterised by distinctive layer structures and narrow band gaps, rendering them suitable for photocatalytic and photoelectrocatalytic applications. The g-C_3N_4/BiOF heterojunction was synthesised using an ultrasonication process and explored as photoanode material in PEC water splitting.[270] Under light illumination, the photoinduced electrons were transferred to the CB of BiOF from the CB of g-C_3N_4. Simultaneously, the holes moved from the VB of BiOF toward the VB of g-C_3N_4. The optimized 6%g-C_3N_4/BiOF electrode showed excellent photoelectrochemical water splitting performance with wastewater rejected from reverse osmosis. The improved PEC performances of g-C_3N_4/BiOI[95,98,271,272] and BiOBr[163] as photoanode materials were investigated. The synergistic trap passivation and charge separation at the g-C_3N_4-S/BiOI heterojunction resulted in a higher photocurrent because of lower charge transfer resistance.[98] The exfoliation *via* the breakage of hydrogen bonds between the sheets and increased crystallinity led to better charge transportation. The integration of Ni as a cocatalyst into the g-C_3N_4 framework enhanced the photocurrent density by minimising the activation energy barrier and enhancing the charge separation and transportation.[163] The introduction of dopant ions (Nd^{3+}) influenced the microstructural, optical and photoelectrochemical properties of C_3N_4 and the heterojunction with BiOI showed considerable improvement in the PEC water splitting performance.[273]

Ultrathin g-C_3N_4 nanolayers were used as the co-catalyst to boost the OER of Bi_2MoO_6 nanosheet arrays with exposed (010) facets.[274] The high surface area, exposed oxygen atoms and even electron transport pathways facilitate charge separation resulting in enhanced PEC performance. Li *et al.* demonstrated the fabrication of a direct Z-scheme heterojunction by encapsulation of the Bi_2O_3/$BiPO_4$ p–n junction in the g-C_3N_4 framework.[275] A new perception of interface engineering was attempted by introducing the nuclear fuel ThO_2 onto g-C_3N_4 for the water-splitting application. The presence of thorium nitrate during g-C_3N_4 polymerisation altered the structure and morphology, improving the PEC stability of the photoanode.[276] Zheng *et al.* reported a plasma-assisted liquid-based fabrication of the g-C_3N_4/Mn_2O_3 p–n heterojunction, which led to the accumulation of electrons and holes in the VB of g-C_3N_4 and CB of Mn_2O_3, respectively.[277] Ag–Ni alloy particles were homogeneously distributed throughout the g-C_3N_4 matrix using an *in situ* solid-state heat treatment, as evidenced by the TEM images. This was the first demonstration of the efficient tuning of the photoelectrochemical properties of g-C_3N_4 photoanodes by incorporating bimetallic alloy particles.[278]

Chen *et al.* synthesised a vertically aligned Si nanowire (NW)/g-C_3N_4 core–shell array using metal-catalysed electroless etching, liquid atomic layer deposition, and annealing methods. The photoelectrode exhibited an extended optical absorption range and significantly improved the PEC performance in comparison with the bulk phase g-C_3N_4.[279] Enhanced visible light absorbance and reduced photogenerated charge recombination in g-C_3N_4/SiC synthesised *via* pulsed laser ablation in liquid was evidenced by absorption and photoluminescence spectra and this contributed to the improved photoelectrochemical activity of the g-C_3N_4/SiC-based photoanode.[280] A direct Z-scheme $NiTiO_3$/g-C_3N_4 heterojunction with enhanced activity under white LED activation was assembled by a simple calcination method.[281] Polydisperse cobalt phosphide nanoparticles were deposited over g-C_3N_4 to form a CoP–CN heterostructure with strong intimate interfacial contact, charge transfer efficiency and stronger photoreductive capability.[282,283] A synergistic effect between the Pt nanoparticles and CoP over the g-C_3N_4 nanosheets contributed to highly boosted photo/electrochemical activity.[283] Islam *et al.* demonstrated the superior performance and stability of the thermolytically fabricated g-C_3N_4/$ZnGa_{1.9}Al_{0.1}O_4$ heterojunction as compared to a hydrolytically prepared counterpart.[284] A nanoengineering approach to the construction of an integrated 3D photoanode comprised of a 1D/2D Ba-doped TaON array and 2-D g-C_3N_4 nanosheets decorated with CoO_x nanoparticles by an innovative stack design, generating a photocurrent of 4.57 mA cm^{-2} at 1.23 V_{RHE} under AM 1.5 simulated sunlight, has been proposed.[285] Table 1 presents a concise comparative evaluation of the PEC performance of g-C_3N_4-based photoanodes.

3.2 Graphitic carbon nitride and its composites as photocathodes

Investigations on photocathodes are rather limited and the most explored systems include Cu_2O,[124,286,287] and CuO.[118,288,289] Cu_2O is a typical p-type narrow band gap (~2 eV) semiconductor with a theoretical photocurrent of −14.7 mA cm^{-2} for water splitting and a solar to hydrogen conversion efficiency of 18.1% on the AM 1.5 spectrum.[290] Due to specific band alignments at an effective heterojunction, the photoexcited electrons in the CB of Cu_2O can transfer to the CB of g-C_3N_4 while the photoexcited holes can transfer from the VB of g-C_3N_4 to the VB of Cu_2O. The PEC performance graphs and schematic pathway for photoelectron excitation and transfer in the Cu_2O/g-C_3N_4 under visible light irradiation are depicted in Fig. 8.[124] The efficiency and stability of the Cu_2O foam photoelectrode could be enhanced by combining it with g-C_3N_4 as a protection layer to alleviate the photocorrosion.[287] With the tactical combination of type II band edge heterojunctions and passivation using g-C_3N_4, a photocathode (Cu_2O/g-C_3N_4/CoS) with high stability was fabricated by Kunturu *et al.*[291] The enhanced light-to-electricity conversion efficiency of the Cu_2O/g-C_3N_4 p–n junction was also utilised to form a triple-layer photocathode Cu_2O/g-C_3N_4/WS_2.[286] The mixed-phase WS_2 nanosheets obtained *via* Li intercalation served as an operative hydrogen evolution catalyst along with enacting the function of an electron acceptor to facilitate electron–hole separation.

A 3D hierarchical C-doped CuO/g-C_3N_4 nanocomposite synthesised by a facile *in situ* microwave-assisted one-pot process yielded CuO nanosheets assembled into unique microflower/dandelion morphologies.[288] High photocorrosion stability, extensive visible light absorption, and excellent PEC performance by CuO/g-C_3N_4 nanocomposites, aided by efficient charge segregation and transfer at the electrode–electrolyte interface and high surface area, have been reported.[118,288,289]

Visible light-aided hydrogen production by PEC water splitting was successfully achieved by the direct synthesis of g-C_3N_4

Table 1 PEC performance of g-C_3N_4-based photoanodes

System	Photocurrent density (mA cm^{-2})	Potential	Electrolyte	Ref.
BCN-0.6	0.055	1.23 V_{RHE}	0.2 M Na_2SO_4 + 0.05 M Na_2S	72
Ph-CN_{600}	0.06	$V_{Ag/AgCl}$	0.1 M KOH	73
Ag/g-C_3N_4 (1 : 10)	0.00640	V_{SCE}	0.05 M Na_2SO_4	74
Ni–CN_x	0.0698	0.26 $V_{Ag/AgCl}$	0.1 M KOH	75
WO_3/g-C_3N_4	0.82	1.23 V_{RHE}	0.5 M Na_2SO_4	81
Co–g-CN	3.253	$V_{Ag/AgCl}$	0.1 M Na_2SO_4	84
BiOI/g-C_3N_4	0.0815	$V_{Ag/AgCl}$	1 M KOH	95
g-C_3N_4–S/BiOI	0.70	$V_{Ag/AgCl}$	0.1 M Na_2SO_4	98
0.8%Y:ZnO@PCN	0.4	1.23 V_{RHE}	Na_2SO_4	100
g-C_3N_4	0.0014	$V_{Ag/AgCl}$	0.5 M Na_2SO_4	101
SCN-27.4	0.468	0.6 $V_{Ag/AgCl}$	0.2 M Na_2SO_4	102
Ti^{3+}–TiO_2/O–g-C_3N_4	0.0034	$V_{Ag/AgCl}$	0.1 M Na_2SO_4	103
0.5 g-C_3N_4/Ti–Fe_2O_3	2.55	$V_{Ag/AgCl}$	1 M NaOH	104
g-C_3N_4/$BiVO_4$	0.42	V_{RHE}	0.5 M Na_2SO_4	105
C_{PVP}/g-C_3N_4	0.00664	V_{SCE}	0.5 M Na_2SO_4	113
CN/BV-1	0.44	0.56 V_{RHE}	0.5 M PBS + Na_2SO_3	114
CN-r$GO_{0.5}$	0.072	1.23 V_{RHE}	0.1 M KOH	116
g-CN600	0.12	1.55 V_{RHE}	0.1 M Na_2SO_4 + 0.1 M Na_2SO_3 + 0.01 M Na_2S	129
g-CN	0.062	1.23 V_{RHE}	0.1 M Na_2SO_4	130
CMD5	0.1	1.55 V_{RHE}	0.1 M Na_2SO_4 + 0.1 M Na_2SO_3 + 0.01 M Na_2S	131
g-CN400	0.075	1.23 V_{RHE}	0.1 M Na_2SO_4 + 0.1 M Na_2SO_3 + 0.01 M Na_2S	132
g-C_3N_4	0.089	1.1 V_{RHE}	0.1 M Na_2SO_4	133
TiO_2/CMB	1.4	$V_{Ag/AgCl}$	0.1 M Na_2S	134
S-BCN	0.1032	1.23 V_{RHE}	0.1 M Na_2SO_4	137
CN@FTO	0.030	1.23 V_{RHE}	0.1 M Na_2SO_4	144
CN-h	0.0035	0.6 V_{SCE}	0.2 M Na_2SO_4	147
CN	0.116	1.23 V_{RHE}	0.1 M KOH	151
Exfoliated g-C_3N_4	0.01021	$V_{Ag/AgCl}$	0.5 M Na_2SO_4	152
CN_T	0.266	1.23 V_{RHE}	0.1 M KOH	153
g-CN PNR	0.1205	1.23 V_{RHE}	0.1 M Na_2SO_4	154
PCN	0.100	1.23 V_{RHE}	1 M NaOH	155
1D-S–C_3N_4	0.010	1 V_{SCE}	0.1 M Na_2SO_4	157
Co/S–C_3N_4/BiOCl	0.393	1.23 V_{RHE}	0.5 M KCl + KH_2PO_4	158
P–C_3N_4/TiO_2	1.98	0 $V_{Ag/AgCl}$	1 M NaOH	159
BCN/TiO_2	1.01	1.23 V_{RHE}	1 M NaOH	160
CN/BCN	0.62	1.23 V_{RHE}	0.1 M Na_2SO_4	161
Ni/S-gC_3N_4/BiOBr	0.177	1.23 V_{RHE}	0.5 M Na_2SO_3 + $NaHCO_3$	163
Ni/g-C_3N_4@CuS	15.5	V_{RHE}	0.1 M KOH	164
Bi@g-C_3N_4/GO	0.3	1.23 V_{RHE}	0.5 M Na_2SO_4	165
P/g-C_3N_4	0.00025	1.2 $V_{Ag/AgCl}$	0.5 M Na_2SO_4	166
V doped g-C_3N_4	0.80	V_{RHE}	0.1 M KOH	167
TiO_2@Co–C_3N_4	1.79	1.23 V_{RHE}	0.1 M Na_2SO_4	168
Pd@g-C_3N_4	0.0788	1.23 V_{RHE}	0.1 M Na_2SO_4	169
GCNML	0.12	1.23 V_{RHE}	0.5 M Na_2SO_4	171
CN-CNT	0.075	1 $V_{Ag/AgCl}$	0.5 M Na_2SO_4	174
pCN/C dots	0.038	1 V_{RHE}	5% v/v TEOA + 0.5 M Na_2SO_4	175
TiO_2/C_3N_4-CMT	2.74	1.23 V_{RHE}	NaOH	176
$CT_{5.0}$	1.481	$V_{Ag/AgCl}$	0.5 M Na_2S	179
C_3N_4–TiO_2	1.5	V_{RHE}	0.25 M Na_2S + 0.35 M Na_2SO_3	180
PCN-TNA	1.42	1.23 V_{RHE}	0.2 M Na_2SO_3	181
TNT-L	0.87	0 $V_{Ag/AgCl}$	1 M KOH	182
g-C_3N_4/TNTAS	0.86	0.7 $V_{Ag/AgCl}$	0.1 M Na_2SO_4	184
TiO_2-4 h/g-CN	0.0433	0.6 V_{SCE}	0.2 M Na_2SO_4	185
20-gCN@TiO_2	0.0723	1.23 V_{RHE}	1 M KOH	186
0D/1D g-C_3N_4/0 V-TiO_2	0.72	1.23 V_{RHE}	0.1 M Na_2SO_4	187
CN QDs/TiO_2	1.34	0.3 $V_{Ag/AgCl}$	0.1 M Na_2SO_4	188
g-C_3N_4 QDs/TNTAs	0.62	0.6 V_{SCE}	0.1 M Na_2SO_4	189
$CNB_{0.15}$ QD@TiO_2	0.57	1.23 V_{RHE}	0.5 M Na_2SO_4	190
d-FCNs-$_{21.59}$/TiO_2	0.1219	1.23 V_{RHE}	0.5 M Na_2SO_4	192
g-C_3N_4/TiO_2	0.1427	1.23 V_{RHE}	1 M KOH	193
TNR@C_N–C_3N_4/FTO	0.64	1.5 $V_{Ag/AgCl}$	0.1 M Na_2SO_4	194
g-C_3N_4/TNAs	0.206	0.63 V_{RHE}	1 M Na_2SO_4	195
CNT70	9.33 mA	1.49 $V_{Ag/AgCl}$	1 M Na_2SO_4	196
2D-B-CN-4	1.63	V_{RHE}	0.1 M Na_2SO_4	197
CNF;TNR-4h	0.18	0.6 $V_{Ag/AgCl}$	0.1 M KOH	198
g-C_3N_4@TiO_2@Co–Pi	1.6	1.23 V_{RHE}	0.1 M Na_2SO_4	199
g-C_3N_4/TiO_2/Co–Pi	0.346	1.1 V_{RHE}	0.1 M Na_2SO_4	200
TiO_2@Co–C_3N_4	1.79	1.23 V_{RHE}	0.1 M Na_2SO_4	201
TiO_2/CuNi@g-C_3N_4	0.890	1.5 V_{RHE}	1 M NaOH	202
CDs/UNC/TiO_2	1.43	1.23 V_{RHE}	1 M NaOH	203

Table 1 (*continued*)

System	Photocurrent density (mA cm^{-2})	Potential	Electrolyte	Ref.
TiO_2/C_3N_4/CNT	2.94	0.6 $V_{Ag/AgCl}$	0.5 M Na_2SO_4	204
CPCT2	1.58	1.23 V_{RHE}	0.5 M Na_2SO_4	205
g-C_3N_4/Fe_2O_3	0.78	$V_{Ag/AgCl}$	1 M NaOH	206
Fe_2O_3/R–CN/Co–Pi	0.7	1.23 V_{RHE}	1 M NaOH	208
WRCN/hematite/Co–Pi	2.14	1.23 V_{RHE}	1 M NaOH	209
$CoFeO_x$/HD–CN	0.60	1.23 V_{RHE}	0.1 M NaOH	210
CoNi–tC_3N_4/a-Fe_2O_3	2.73	1.23 V_{RHE}	1 M NaOH	212
Ti:Fe_2O_3@GCNNs	2.75	1.23 V_{RHE}	0.1 M KOH	213
Gcncsf	0.0238	$V_{Ag/AgCl}$	Na_2SO_4	214
NCD@CNFO	3.07	V_{RHE}	0.1 M Na_2SO_4	215
g-C_3N_4/WO_3	1.48	2 V_{RHE}	0.2 M Na_2SO_4	216
WO_3/g-C_3N_4 NSAs	0.73	1.23 V_{RHE}	Seawater	217
g-C_3N_4/WO_3	1.92	1.23 V_{RHE}	0.1 M KH_2PO_4	218
g-C_3N_4/Pt/ZnO	0.120	0.5 $V_{Ag/AgCl}$	0.5 M Na_2SO_4	219
1 D ZnO/g-C_3N_4	0.12	V_{RHE}	0.5 M Na_2SO_4	220
ZnO/ZnS/g-C_3N_4	0.66	1.23 V_{RHE}	0.5 M Na_2SO_4	221
ZnO/g-C_3N_4	0.25	1.23 V_{RHE}	1 M KOH	222
ZnO/C_3N_4-10	1.68	1.19 V_{RHE}	0.5 M Na_2SO_4	223
Co–Pi/CNNs/ZnO	2.45	1.23 V_{RHE}	0.2 M Na_2SO_4	224
Co–Pi/g-C_3N_4@ZnO	5	1.23 V_{RHE}	3.5 wt% NaCl	225
CdS/g-C_3N_4/ZnO	3.34	1.23 V_{RHE}	0.1 M Na_2S + 0.2 M Na_2SO_3	226
ZnO/α-Fe_2O_3/g-C_3N_4	0.97	1.23 V_{RHE}	1 M NaOH	227
g-C_3N_4/SnO_2	1.82	0.2 $V_{Ag/AgCl}$	0.1 M NaOH	228
CNAs-20	3.93	1 $V_{Ag/AgCl}$	0.1 M Na_2SO_4	229
g-C_3N_4@1/8NiO	20.0	1.23 V_{RHE}	0.5 M H_2SO_4	230
NiO@g-CN	0.00865	0.7 V_{SCE}	0.5 M Na_2SO_4	231
BWO QDs/CN	0.00039	1.23 V_{RHE}	0.2 M Na_2SO_4	232
SCN/BWO	0.0574	1.23 V_{RHE}	1 M KOH	233
CZO	0.162	$V_{Ag/AgCl}$	0.1 M Na_2SO_3	235
g-C_3N_4–$BiVO_4$	0.00202	1.23 V_{RHE}	1 M KOH	236
$BiVO_4$/g-C_3N_4	1.14	1.23 V_{RHE}	0.5 M Na_2SO_4 buffered with a 1 M Na_2SO_3	237
BV/CN-5	0.7	1.23 V_{RHE}	0.5 M Na_2SO_4	239
$BiVO_4$/g-C_3N_4-NS	3.12	1.23 V_{RHE}	0.1 M Na_2SO_4	240
g-C_3N_4/Mo:$BiVO_4$	3.11	1.23 V_{RHE}	0.1 M KH_2PO_4	241
$NiFeO_x$/B-C_3N_4/Mo:$BiVO_4$	5.93	1.23 V_{RHE}	PPB	242
γ-g-C_3N_4@$BiVO_4$	1.38	$V_{Ag/AgCl}$	0.5 M Na_2SO_4	243
g-$C_3N_4/BiVO_4$(30%)	0.00046	$V_{Ag/AgCl}$	0.1 M Na_2SO_4	244
$BiVO_4$/g-CN	7.4	2.2 V_{RHE}	0.1 M KH_2PO_4 + 1 M Na_2SO_3	245
$C_3N_4/InVO_4$	0.013	0.9 $V_{Ag/AgCl}$	0.1 M Na_2SO_4	246
$FeVO_4/C_3N_4$	0.18	0.7 V_{SCE}	0.1 M Na_2SO_4	247
mt-CN/MoS_2	0.16	0.5 $V_{Ag/AgCl}$	0.1 M Na_2SO_4	251
MoS_2/g-C_3N_4	0.07	−0.8 $V_{Ag/AgCl}$	0.1 M H_2SO_4	252
g-C_3N_4/Bi_2S_3/BiNPs	7.11	1.23 V_{RHE}	0.1 M Na_2SO_4 + 0.1 M Na_2SO_3	253
CNIS25	0.0078	1.5 $V_{Ag/AgCl}$	0.1 M Na_2SO_3	254
In_2S_3/S–C_3N_4-dots-20	4.93	1.18 V_{RHE}	3.5 wt% NaCl solution and Na_2SO_4	255
g-C_3N_4/CdS	5.4	0.2 $V_{Ag/AgCl}$	0.5 M Na_2S + 0.5 M Na_2SO_3	256
Ag@g-C_3N_4/ZnS	0.2	1.60 V_{RHE}	1 M KOH	257
DPCN/NRGO/NiFe-LDH	0.1623	1.4 V_{RHE}	0.01 M Na_2SO_4	261
CoMn-LDH/g-C_3N_4	0.227	$V_{Ag/AgCl}$	1 M KOH	262
CoFe-LDH@g-C_3N_4	0.196	V_{RHE}	1 M KOH	263
CNN G3 LDH	0.97	0.61 $V_{Ag/AgCl}$	0.1 M Na_2SO_4	265
CuTi-LDH/C_3N_4	0.014	V_{RHE}	1 M KOH	266
C_3N_4@CuAF/$Ni(OH)_2$	0.32	1.23 V_{RHE}	0.5 M Na_2SO_4	268
6%g-C_3N_4/BiOF	0.0482	1.23 V_{RHE}	0.5 M NaOH	270
6%g-C_3N_4/BiOI	0.1316	V_{RHE}	0.5 M Na_2SO_3 + $NaHCO_3$	271
Nd:g-C_3N_4/BiOI	1.55	1.23 V_{RHE}	0.5 M Na_2SO_4	273
Bi_2MoO_6/g-C_3N_4	0.520	0.7 V_{SCE}	0.1 M Na_2SO_4	274
g-$C_3N_4/Bi_2O_3/BiPO_4$	0.095	1.25 $V_{Ag/AgCl}$	0.1 M Na_2SO_4	275
g-C_3N_4/ThO_2	0.00971	1.23 $V_{Ag/AgCl}$	0.5 M Na_2SO_4	276
CN/Mn_2O_3/FTO	0.093	0.8 V_{RHE}	0.1 M Na_2SO_4	277
AgNi/g-C_3N_4	1.29	1 $V_{Ag/AgCl}$	1.0 M NaOH	278
SiNWs/g-C_3N_4	0.045	0 V_{Pt}	0.5 M Na_2SO_4	279
g-C_3N_4/SiC	0.015	V_{SCE}	0.5 M Na_2SO_4	280
CoP-CN	0.15	0.4 $V_{Ag/AgCl}$	0.5 M Na_2SO_4	282
CoOx/C_3N_4/Ba–TaON	4.57	1.23 V_{RHE}	1 M NaOH	285

films on a polycrystalline $CuInS_2$ chalcopyrite substrate.[292] The electrode showed good activity and stability with g-C_3N_4 acting as a protective layer for semiconducting $CuInS_2$, inhibiting degradation and photo-corrosion under acidic conditions.

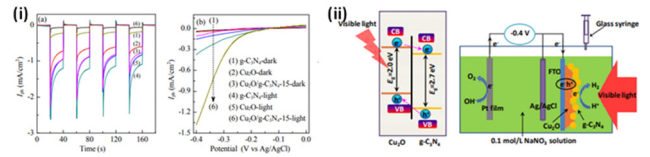

Fig. 8 (i) (a) Transient photocurrent response at a bias potential of −0.4 V (*vs.* Ag/AgCl) under visible light: [(1) Cu_2O; (2) Cu_2O/g-C_3N_4-5; (3) Cu_2O/g-C_3N_4-10; (4) Cu_2O/g-C_3N_4-15; (5) Cu_2O/g-C_3N_4-20; (6) g-C_3N_4]. (b) Linear sweep voltammograms of Cu_2O, g-C_3N_4 and Cu_2O/g-C_3N_4-15 films in the dark and under visible light. (ii) Schematic pathway for photoelectron transfer and the photoelectrochemical process in Cu_2O/g-C_3N_4 film under visible light irradiation. Reprinted from ref. 151 with permission.

While the solar spectral range up to 460 nm was captured by the high band gap g-C_3N_4 material, the red portion was absorbed by the low band gap $CuInS_2$ (~1.5 eV) semiconducting electrode with a smaller band gap. The generation of cathodic photocurrents with an onset potential of +0.21 V_{RHE} in 0.1 M H_2SO_4 aqueous solution was observed over polycrystalline $CuInS_2$, and the introduction of C_3N_4 enhanced the onset potential to 0.36 V_{RHE}. The design and development of a $C_3N_{4-x}S_{3x/2}$/CdS/$CuIn_{0.7}Ga_{0.3}S_2$ photocathode with optimally aligned energy levels to facilitate photoactivity was undertaken by Wang *et al.*[293] The alteration of the CdS/CIGS materials using a stable and band-aligned protecting layer of S-doped C_3N_4 could satisfy the requisites for highly efficient water reduction materials. A molten-salt-based synthetic approach was adopted for the preparation of Cu-modified g-C_3N_4 with superior photocathodic performance on account of the coordination effect of Cu and the formation of a type II heterojunction due to *in situ* generation of CuCl.[294] After the photoexcitation to the CB of coordinated C_3N_4 and then to the CB of CuCl, the electrons were expended for H_2 generation.

Biopolymer-activation of g-CN *via* soft-templating and the incorporation of active carbon-dopant sites was demonstrated by Zhang *et al.*[295] Two biopolymers, alginate and gelatin, were used as activating agents for g-C_3N_4. Synergistic interactions between the g-C_3N_4 precursor and biopolymer precursor induced a sponge-like porosity and simultaneous C doping, leading to enhanced PEC activity. Carbon doping enhances the conjugation, thereby extending the absorption edge. Electric-field-assisted charge transfer at the interfaces has been utilised to construct ZnO nanotube array-decorated g-C_3N_4 particles with improved photocathodic performance.[296] Grafting of $CoSe_2$ nanorods into g-C_3N_4 nanosheets reduced the charge accumulation on $CoSe_2$, providing greater stability. Basu *et al.* reported g-C_3N_4–$CoSe_2$ decorated on p-Si MWs that could function as stable and competent photocathodes for PEC H_2 evolution.[120] The efficient snatching of photogenerated electrons by $CoSe_2$ and the subsequent transfer to the Si surface and the electrolyte explained the high performance. The as-prepared p-Si/C_3N_4–$CoSe_2$ heterostructure could afford a photocurrent density of −4.89 mA cm^{-2} at 0 V_{RHE}. Owing to the more positive valence band potential of g-C_3N_4 relative to NiO, it can act as a cocatalyst and photosensitizer for the NiO photocathode, capable of injecting holes into p-type NiO.[297] The photocathodes exhibited excellent stability in both air and N_2-saturated neutral environments. A 0D/2D $AgVO_3$/g-C_3N_4 photocathode exhibited a high photocurrent density of −1.02 mA cm^{-2} at 0 V_{RHE}.[298] Enhancing the efficiency of the g-C_3N_4 photocathode *via* the o-catalyst decoration technique was attempted by Shanker *et al.*[299] An extended interface for the efficient separation of photoexcited electron–hole pairs through electron transfer from g-C_3N_4 to N graphene–titanium nitride (TiN–NFG) could be achieved in C_3N_4:TiN–NFG nanocrystals. A stable 2D/2D heterojunction g-C_3N_4/graphydine was prepared by simple π–π stacking interactions. The incorporation of Pt nanoparticles on g-C_3N_4 increased the photocurrent.[300] Gopalakrishnan *et al.* reported silicon nanowire-based hybrid nanostructures comprised of $SrTiO_3$ nanoparticle-coupled g-C_3N_4 nanosheets as photocathodes. The hybrid heterojunction

Table 2 PEC performance of g-C_3N_4-based photocathodes

System	Photocurrent density (mA cm^{-2})	Potential	Electrolyte	Ref.
ZnO/Au/g-C_3N_4	−0.29	0 V_{RHE}	0.2 M Na_2SO_4	99
g-C_3N_4/CuO	−0.85	0 V_{RHE}	0.1 M Na_2SO_4	118
Si/C_3N_4–$CoSe_2$-100	−8.4	−0.289 V_{RHE}	0.5 M H_2SO_4	120
Cu_2O/g-C_3N_4	−1.38	−0.4 $V_{Ag/AgCl}$	0.1 M $NaNO_3$	124
Cu_2O/g-C_3N_4/WS_2	−9.5	−0.55 V_{RHE}	1 M Na_2SO_4	286
Cu_2O foam/g-C_3N_4	−2.5	0 V_{RHE}	0.1 M Na_2SO_4	287
C–CuO/CN	−2.85	0 V_{RHE}	0.1 M Na_2SO_4	288
g-C_3N_4/$CuInS_2$	−0.3	−0.6 $V_{Ag/AgCl}$	0.1 M H_2SO_4	292
$C_3N_{4-x}S_{3x/2}$/CdS/CIGS	−5	−0.3 V_{RHE}	1 M K_2HPO_4/KH_2PO_4	293
Cu–CN–W	−0.200	0.42 V_{RHE}	0.2 M Na_2SO_4	294
g-C_3N_4/NiO/FTO	−0.02	0 V_{RHE}	0.1 M Na_2SO_4	297
$AgVO_3$/g-C_3N_4	−1.02	0 V_{RHE}	1 M Na_2SO_4	298
g-C_3N_4:TiN–NFG	−0.196	0.11 V_{RHE}	0.5 M Na_2SO_4 and 10 vol% TEOA	299
Pt@g-C_3N_4/GDY	−0.133	0 V_{NHE}	0.1 M Na_2SO_4	300
Hybrid Si NWs@g-C_3N_4 NSs–$SrTiO_3$ NPs	−28	1.23 V_{RHE}	0.5 M Na_2SO_4	301
g-C_3N_4:ITO	−0.070	1 V_{RHE}	0.5 M Na_2SO_4	302
CN/TO/PTO film	−0.0685	0 $V_{Ag/AgCl}$	0.1 M Na_2SO_4	304
$LaFeO_3$/g-C_3N_4	−0.004	−0.3 $V_{Ag/AgCl}$	0.1 M Na_2SO_4	305
ZnSe/g-C_3N_4	−0.5	$V_{Ag/AgCl}$	0.5 M Na_2SO_4	306
h-PCN	−0.1	V_{RHE}	0.5 M H_2SO_4	307

photocathode exhibited a photocurrent density of -28 mA cm^{-2} at neutral pH. The PEC water reduction activity was ascribed to the formation of a built-in potential electrode/electrolyte interface due to charge separation and migration from Si NWs to the interfacial heterojunction layer.[276] With a bias of 0 V_{RHE} in a neutral electrolyte, the Z-scheme ZnO/Au/g-C_3N_4 photocathode exhibited a stable photocurrent of -0.29 mA cm^{-2} in the presence of a Pt co-catalyst. On account of its high work function (-5.30 eV), Au NPs mediated the electron transfer from ZnO to g-C_3N_4, completing a direct Z-scheme charge-carrier process.[301] Shanker *et al.* introduced Sn-doped In_2O_3 (ITO) nanocrystals as co-catalysts for g-C_3N_4, generating a six-fold activity enhancement.[302] A type-II ferroelectric-semiconductor heterojunction of g-C_3N_4 with $BiFeO_3$ has been reported.[303] Another ferroelectric material, $PbTiO_3$ (PTO) when combined with g-C_3N_4 formed Z-scheme heterojunctions with TiO_2 inserted between PTO and g-C_3N_4 to form a buffer layer.[304] The deposition of $LaFeO_3$ at the surface of the g-C_3N_4 film *via* magnetron sputtering followed by oxidation was reported by Gries *et al.*[305] A type-II heterostructure ZnSe/g-C_3N_4 obtained by implanting the ZnSe nanoflowers into the g-C_3N_4 framework aided by ultrasonication was tested for PEC water splitting.[306] The photocurrent enhancement for g-C_3N_4 in the cathodic direction could be achieved by P doping employing trioctylphosphine oxide as a dopant precursor.[307] Table 2 provides the PEC performance of g-C_3N_4-based photocathodes.

4. Conclusion and perspectives

This review delivers a comprehensive depiction of g-C_3N_4-based materials for PEC water splitting. Considering the requirements for the VB and CB positions, g-C_3N_4 can be used both as a photocathode and anode. Nonetheless, its inherent shortcomings such as small surface area, low electrical conductivity and rapid electron–hole recombination limit its PEC activity. In general, the low photocurrent density exhibited by pristine g-C_3N_4 impairs its potential to meet commercial demands. High-quality g-C_3N_4 films are essential for efficient light absorption and charge generation in the PEC water splitting procedure. To achieve maximal activity, the g-C_3N_4 films should be homogeneous, continuous, and in good contact with the substrate. For the synthesis of g-C_3N_4 films, innovative bottom-up methodologies should be used since they mitigate the poor dispersibility and solubility problems of g-C_3N_4, which are often present in top-down approaches for g-C_3N_4 film fabrication.

New hybrid non-vacuum-based synthetic protocols to obtain homogeneous and crack-free films with good adhesion to the conductive substrate should be developed with controllable thickness to fabricate the large surface area thin film photoelectrodes. The process of the synthesis of films should modulate and control the intrinsic π-conjugated structure for g-C_3N_4 light absorption and conversion to be further increased, resulting from substantial alterations to its electronic state, band structure, and optical/electrical characteristics. A few strategies that can be investigated to modulate the intrinsic properties to achieve ideal PEC performance include heteroatom doping, defect engineering, and the introduction of functional groups into the g-C_3N_4 matrix. The controllable changes in functional groups on the surface can improve the investigations and control over the surface plane fabrication, adhesion and charge transfer. Morphological nano levels can also aid in improving the PEC performance. There is ample scope for exploring the impact of various hierarchical nanostructures, including nanoparticles, nanorods, *etc.*, on PEC performance.

The decoration of hole-transporting layers (HTLs) and ETLs (electron-transporting layers) with minimum to no parasitic light absorption should be studied. The stable intermediate layers to avoid the direct contact of electrolyte and light absorbing layer should be of utmost priority for the longevity of the electrode. The investigation of effective oxidation/reduction cocatalysts that align well with the charge capturing from the bulk layers of g-C_3N_4 is essential since the activation energy of water oxidation is the limiting step for overall water splitting. Photo-generated charge carriers can be effectively separated, and their recombination can be suppressed by the cocatalyst by providing specific active surface sites to participate in the reduction and oxidation reaction. To accomplish efficient charge transfer, good interfacial contact between the cocatalyst and g-C_3N_4 must be sustained using buffer layers. The cocatalyst introduction can also reduce the overpotential for the HER and OER. The formation of type-II or Z-scheme heterojunctions with other semiconductors can facilitate high charge mobility, thereby reducing the prospects of electron–hole recombination; the metal oxides, double oxides, and chalcogenides are widely explored in this category. Integration with conductive matrices like graphene improves electronic conductivity and provides channels for electron transfer. The plasmonic effect of the metal nanoparticles loading may be beneficial in widening the light absorption and increasing the charge carrier concentration. Long-term and large-scale applications of g-C_3N_4-based photoelectrodes rely substantially on their stability and feasibility to manufacture large surface area films economically. Additional research on the modified technologies is necessary to ensure a steady run. This includes applying protective layers and achieving strong adherence of g-C_3N_4 films on substrates. Theoretical studies should be taken into consideration for understanding the charge transfer kinetics and mechanism assisting the rational design of systems for efficient PEC water splitting and relieving experimental workload and chemical cost. DFT studies are useful for comprehending the fundamental process of the improvement of PEC activity brought about by different modification techniques at the atomic or unit-cell scale. Clarifying the kinetics of charge transfer in a functional photoelectrode and gaining a thorough grasp of charge transfer and recombination in semiconductor materials is crucial. Consequently, it would be ideal to use *in situ* spectroscopic studies to observe charge transfer kinetics, phase changes, and reactive reaction intermediates in real time. Additional sophisticated spectroscopic

techniques, like time-resolved fluorescence measurements, transient absorption spectroscopy, and time-resolved microwave conductivity, could be useful in elucidating the relevant photoelectrochemical processes. The PEC application of g-C_3N_4 is still in the early phase. With the intensive perpetual research in the field, g-C_3N_4 may emerge as a potential durable system for PEC applications in the coming years.

Author contributions

Merin Joseph: conceptualization, data curation, writing – original draft, Mohit Kumar: writing – reviewing and editing, Suja Haridas: supervision, writing – reviewing and editing, Challapalli Subrahmanyam: supervision, writing – reviewing and editing, Sebastian Nybin Remello: supervision.

Conflicts of interest

There are no conflicts to declare.

Acknowledgements

The financial support from SMNRI funding, UGC-SAP, DST-PURSE, DST-FIST and RUSA 2.0 grants are acknowledged. The fellowships from Cochin University of Science and Technology in Cochin, Kerala, and RUSA 2.0 are also acknowledged.

References

1 C. V. Reddy, K. R. Reddy, N. P. Shetti, J. Shim, T. M. Aminabhavi and D. D. Dionysiou, *Int. J. Hydrogen Energy*, 2020, **45**, 18331–18347.
2 C. Daulbayev, F. Sultanov, B. Bakbolat and O. Daulbayev, *Int. J. Hydrogen Energy*, 2020, **45**, 33325–33342.
3 R. Gao, J. Zhu and D. Yan, Transition metal-based layered double hydroxides for photo (electro) chemical water splitting: a mini review, *Nanoscale*, 2021, **13**(32), 13593–13603.
4 L. Bai, H. Huang, S. Yu, D. Zhang, H. Huang and Y. Zhang, Role of transition metal oxides in g-C_3N_4-based heterojunctions for photocatalysis and supercapacitors, *J. Energy Chem.*, 2022, **64**, 214–235.
5 Y. Wang, L. Liu, T. Ma, Y. Zhang and H. Huang, 2D graphitic carbon nitride for energy conversion and storage, *Adv. Funct. Mater.*, 2021, **31**(34), 2102540.
6 W. Yang, R. R. Prabhakar, J. Tan, S. D. Tilley and J. Moon, Strategies for enhancing the photocurrent, photovoltage, and stability of photoelectrodes for photoelectrochemical water splitting, *Chem. Soc. Rev.*, 2019, **48**(19), 4979–5015.
7 M. A. Desai, A. N. Vyas, G. D. Saratale and S. D. Sartale, Zinc oxide superstructures: recent synthesis approaches and application for hydrogen production via photoelectrochemical water splitting, *Int. J. Hydrogen Energy*, 2019, **44**(4), 2091–2127.
8 M. Ali, E. Pervaiz, U. Sikandar and Y. Khan, A review on the recent developments in zirconium and carbon-based catalysts for photoelectrochemical water-splitting, *Int. J. Hydrogen Energy*, 2021, **46**(35), 18257–18283.
9 T. Higashi, H. Nishiyama, Y. Suzuki, Y. Sasaki, T. Hisatomi, M. Katayama, T. Minegishi, K. Seki, T. Yamada and K. Domen, Transparent Ta3N5 photoanodes for efficient oxygen evolution toward the development of tandem cells, *Angew. Chem., Int. Ed.*, 2019, **58**(8), 2300–2304.
10 M. A. Mushtaq, A. Kumar, G. Yasin, M. Arif, M. Tabish, S. Ibraheem and X. Cai, *et al.*, 3D interconnected porous Mo-doped WO3@ CdS hierarchical hollow heterostructures for efficient photoelectrochemical nitrogen reduction to ammonia, *Appl. Catal., B*, 2022, **317**, 121711.
11 L. Pengyan, T. Zhang, M. A. Mushtaq, S. Wu, X. Xiang and D. Yan, Research progress in organic synthesis by means of photoelectrocatalysis, *Chem. Rec.*, 2021, **21**(4), 841–857.
12 A. Fujishima and K. Honda, Electrochemical photolysis of water at a semiconductor electrode, *Nature*, 1972, **238**(5358), 37–38.
13 A. G. Tamirat, J. Rick, A. A. Dubale, W.-N. Su and B.-J. Hwang, Using hematite for photoelectrochemical water splitting: a review of current progress and challenges, *Nanoscale Horiz.*, 2016, **1**(4), 243–267.
14 P. Peerakiatkhajohn, J.-H. Yun, S. Wang and L. Wang, Review of recent progress in unassisted photoelectrochemical water splitting: from material modification to configuration design, *J. Photonics Energy*, 2017, **7**(1), 012006.
15 P. Subramanyam, T. Vinodkumar, D. Nepak, M. Deepa and C. Subrahmanyam, Mo-doped BiVO4@ reduced graphene oxide composite as an efficient photoanode for photoelectrochemical water splitting, *Catal. Today*, 2019, **325**, 73–80.
16 K. Mika, K. Syrek, T. Uchacz, G. D. Sulka and L. Zaraska, Dark nanostructured ZnO films formed by anodic oxidation as photoanodes in photoelectrochemical water splitting, *Electrochim. Acta*, 2022, **414**, 140176.
17 R.-B. Wei, P.-Y. Kuang, H. Cheng, Y.-B. Chen, J.-Y. Long, M.-Y. Zhang and Z.-Q. Liu, Plasmon-enhanced photoelectrochemical water splitting on gold nanoparticle decorated ZnO/CdS nanotube arrays, *ACS Sustainable Chem. Eng.*, 2017, **5**(5), 4249–4257.
18 P. Kumar, P. Sharma, R. Shrivastav, S. Dass and V. R. Satsangi, Electrodeposited zirconium-doped α-Fe_2O_3 thin film for photoelectrochemical water splitting, *Int. J. Hydrogen Energy*, 2011, **36**(4), 2777–2784.
19 G. Wang, H. Wang, Y. Ling, Y. Tang, X. Yang, R. C. Fitzmorris, C. Wang, J. Z. Zhang and Y. Li, Hydrogen-treated TiO_2 nanowire arrays for photoelectrochemical water splitting, *Nano Lett.*, 2011, **11**(7), 3026–3033.
20 V. Cristino, S. Caramori, R. Argazzi, L. Meda, G. L. Marra and C. A. Bignozzi, Efficient photoelectrochemical water splitting by anodically grown WO_3 electrodes, *Langmuir*, 2011, **27**(11), 7276–7284.
21 Z. Liu, X. Lu and D. Chen, Photoelectrochemical water splitting of CuInS2 photocathode collaborative modified with separated catalysts based on efficient photogenerated electron–hole separation, *ACS Sustainable Chem. Eng.*, 2018, **6**(8), 10289–10294.

22 D. Sharma, S. Upadhyay, V. R. Satsangi, R. Shrivastav, U. V. Waghmare and S. Dass, Improved photoelectrochemical water splitting performance of $Cu_2O/SrTiO_3$ heterojunction photoelectrode, *J. Phys. Chem. C*, 2014, **118**(44), 25320–25329.

23 S. Bai, J. Han, K. Zhang, Y. Zhao, R. Luo, D. Li and A. Chen, rGO decorated semiconductor heterojunction of $BiVO_4$/NiO to enhance PEC water splitting efficiency, *Int. J. Hydrogen Energy*, 2022, **47**(7), 4375–4385.

24 H. She, M. Jiang, P. Yue, J. Huang, L. Wang, J. Li, G. Zhu and Q. Wang, Metal (Ni^{2+}/Co^{2+}) sulfides modified $BiVO_4$ for effective improvement in photoelectrochemical water splitting, *J. Colloid Interface Sci.*, 2019, **549**, 80–88.

25 S. Chandrasekaran, L. Yao, L. Deng, C. Bowen, Y. Zhang, S. Chen, Z. Lin, F. Peng and P. Zhang, Recent advances in metal sulfides: from controlled fabrication to electrocatalytic, photocatalytic and photoelectrochemical water splitting and beyond, *Chem. Soc. Rev.*, 2019, **48**(15), 4178–4280.

26 N. Han, P. Liu, J. Jiang, L. Ai, Z. Shao and S. Liu, Recent advances in nanostructured metal nitrides for water splitting, *J. Mater. Chem. A*, 2018, **6**(41), 19912–19933.

27 M. Wu, Q. Wang, Q. Sun and P. Jena, Functionalized graphitic carbon nitride for efficient energy storage, *J. Phys. Chem. C*, 2013, **117**(12), 6055–6059.

28 Y. Luo, Y. Yan, S. Zheng, H. Xue and H. Pang, Graphitic carbon nitride based materials for electrochemical energy storage, *J. Mater. Chem. A*, 2019, **7**(3), 901–924.

29 A. Thomas, A. Fischer, F. Goettmann, M. Antonietti, J.-O. Müller, R. Schlögl and J. M. Carlsson, Graphitic carbon nitride materials: variation of structure and morphology and their use as metal-free catalysts, *J. Mater. Chem.*, 2008, **18**(41), 4893–4908.

30 X. Wang, K. Maeda, A. Thomas, K. Takanabe, G. Xin, J. M. Carlsson, K. Domen and M. Antonietti, A metal-free polymeric photocatalyst for hydrogen production from water under visible light, *Nat. Mater.*, 2009, **8**(1), 76–80.

31 Y. Zhang, J. Liu, G. Wu and W. Chen, Porous graphitic carbon nitride synthesized via direct polymerization of urea for efficient sunlight-driven photocatalytic hydrogen production, *Nanoscale*, 2012, **4**(17), 5300–5303.

32 G. Liu, G. Zhao, W. Zhou, Y. Liu, H. Pang, H. Zhang and D. Hao, *et al.*, In situ bond modulation of graphitic carbon nitride to construct p–n homojunctions for enhanced photocatalytic hydrogen production, *Adv. Funct. Mater.*, 2016, **26**(37), 6822–6829.

33 Q. Liang, Z. Li, Z.-H. Huang, F. Kang and Q.-H. Yang, Holey graphitic carbon nitride nanosheets with carbon vacancies for highly improved photocatalytic hydrogen production, *Adv. Funct. Mater.*, 2015, **25**(44), 6885–6892.

34 M. Wei, L. Gao, J. Li, J. Fang, W. Cai, X. Li and A. Xu, Activation of peroxymonosulfate by graphitic carbon nitride loaded on activated carbon for organic pollutants degradation, *J. Hazard. Mater.*, 2016, **316**, 60–68.

35 D. Rattan Paul and S. P. Nehra, Graphitic carbon nitride: a sustainable photocatalyst for organic pollutant degradation and antibacterial applications, *Environ. Sci. Pollut. Res.*, 2021, **28**, 3888–3896.

36 J. Mao, T. Peng, X. Zhang, K. Li, L. Ye and L. Zan, Effect of graphitic carbon nitride microstructures on the activity and selectivity of photocatalytic CO_2 reduction under visible light, *Catal. Sci. Technol.*, 2013, **3**(5), 1253–1260.

37 P. Xia, B. Zhu, J. Yu, S. Cao and M. Jaroniec, Ultra-thin nanosheet assemblies of graphitic carbon nitride for enhanced photocatalytic CO_2 reduction, *J. Mater. Chem. A*, 2017, **5**(7), 3230–3238.

38 Y. Zhang and M. Antonietti, Photocurrent generation by polymeric carbon nitride solids: an initial step towards a novel photovoltaic system, *Chem. – Asian J.*, 2010, **5**(6), 1307–1311.

39 L. Wang, Y. Tong, J. Feng, J. Hou, J. Li, X. Hou and J. Liang, G-C_3N_4-based films: A rising star for photoelectrochemical water splitting, *Sustainable Mater. Technol.*, 2019, **19**, e00089.

40 X. Zou, Z. Sun and Y. H. Hu, g-C_3N_4-based photoelectrodes for photoelectrochemical water splitting: A review, *J. Mater. Chem. A*, 2020, **8**(41), 21474–21502.

41 L. Wang, W. Si, Y. Tong, F. Hou, D. Pergolesi, J. Hou, T. Lippert, S. X. Dou and J. Liang, Graphitic carbon nitride (g-C_3N_4)-based nanosized heteroarrays: promising materials for photoelectrochemical water splitting, *Carbon Energy*, 2020, **2**(2), 223–250.

42 R. Koutavarapu, S. G. Peera, T. G. Lee, C. R. Myla, D.-Y. Lee, J. Shim and S. K. Balasingam, Recent trends in graphitic carbon nitride-based binary and ternary heterostructured electrodes for photoelectrochemical water splitting, *Processes*, 2021, **9**(11), 1959.

43 J. Safaei, N. A. Mohamed, M. F. M. Noh, M. F. Soh, N. A. Ludin, M. A. Ibrahim, W. N. R. W. Isahak and M. A. M. Teridi, Graphitic carbon nitride (g-C3N4) electrodes for energy conversion and storage: a review on photoelectrochemical water splitting, solar cells and supercapacitors, *J. Mater. Chem. A*, 2018, **6**(45), 22346–22380.

44 W. Xiong, F. Huang and R.-Q. Zhang, Recent developments in carbon nitride based films for photoelectrochemical water splitting, *Sustainable Energy Fuels*, 2020, **4**(2), 485–503.

45 M. Volokh, G. Peng, J. Barrio and M. Shalom, Carbon nitride materials for water splitting photoelectrochemical cells, *Angew. Chem., Int. Ed.*, 2019, **58**(19), 6138–6151.

46 N. Z. Muradov and T. N. Veziroğlu, "Green" path from fossil-based to hydrogen economy: an overview of carbon-neutral technologies, *Int. J. Hydrogen Energy*, 2008, **33**(23), 6804–6839.

47 S. S. Penner, Steps toward the hydrogen economy, *Energy*, 2006, **31**(1), 33–43.

48 G. Marbán and T. Valdés-Solís, Towards the hydrogen economy?, *Int. J. Hydrogen Energy*, 2007, **32**(12), 1625–1637.

49 T. Grewe, M. Meggouh and H. Tueysuez, Nanocatalysts for solar water splitting and a perspective on hydrogen economy, *Chem. – Asian J.*, 2016, **11**(1), 22–42.

50 W. C. Nadaleti, E. G. de Souza and S. N. M. de Souza, The potential of hydrogen production from high and low-temperature electrolysis methods using solar and nuclear energy sources: The transition to a hydrogen economy in Brazil, *Int. J. Hydrogen Energy*, 2022, **47**(82), 34727–34738.

51 M.-K. Kazi, F. Eljack, M. M. El-Halwagi and M. Haouari, Green hydrogen for industrial sector decarbonization: Costs and impacts on hydrogen economy in qatar, *Comput. Chem. Eng.*, 2021, **145**, 107144.
52 J. Joy, J. Mathew and S. C. George, Nanomaterials for photoelectrochemical water splitting–review, *Int. J. Hydrogen Energy*, 2018, **43**(10), 4804–4817.
53 M. A. Marwat, M. Humayun, M. W. Afridi, H. Zhang, M. R. Abdul Karim, M. Ashtar and M. Usman, *et al.*, Advanced catalysts for photoelectrochemical water splitting, *ACS Appl. Energy Mater.*, 2021, **4**(11), 12007–12031.
54 M. Joseph and S. Haridas, Recent progresses in porphyrin assisted hydrogen evolution, *Int. J. Hydrogen Energy*, 2020, **45**(21), 11954–11975.
55 P. Subramanyam, B. Meena, V. Biju, H. Misawa and S. Challapalli, Emerging materials for plasmon-assisted photoelectrochemical water splitting, *J. Photochem. Photobiol., C*, 2022, **51**, 100472.
56 Y.-H. Chiu, T.-H. Lai, M.-Y. Kuo, P.-Y. Hsieh and Y.-J. Hsu, Photoelectrochemical cells for solar hydrogen production: Challenges and opportunities, *APL Mater.*, 2019, **7**(8), 1–11.
57 H. Song, S. Luo, H. Huang, B. Deng and J. Ye, Solar-driven hydrogen production: Recent advances, challenges, and future perspectives, *ACS Energy Lett.*, 2022, **7**(3), 1043–1065.
58 Y. Asakura, T. Higashi, H. Nishiyama, H. Kobayashi, M. Nakabayashi, N. Shibata and T. Minegishi, *et al.*, Activation of a particulate Ta 3 N 5 water-oxidation photoanode with a GaN hole-blocking layer, *Sustainable Energy Fuels*, 2018, **2**(1), 73–78.
59 S. Akiyama, M. Nakabayashi, N. Shibata, T. Minegishi, Y. Asakura, M. Abdulla-Al-Mamun and T. Hisatomi, *et al.*, Highly efficient water oxidation photoanode made of surface modified LaTiO2N particles, *Small*, 2016, **12**(39), 5468–5476.
60 W.-T. Qiu, Y.-C. Huang, Z.-L. Wang, S. Xiao, H.-B. Ji and Y.-X. Tong, Effective strategies towards high-performance photoanodes for photoelectrochemical water splitting, *Acta Phys.-Chim. Sin.*, 2017, **33**(1), 80–102.
61 E. A. Kraut, R. W. Grant, J. R. Waldrop and S. P. Kowalczyk, Precise determination of the valence-band edge in x-ray photoemission spectra: application to measurement of semiconductor interface potentials, *Phys. Rev. Lett.*, 1980, **44**(24), 1620.
62 Q. Jia, K. Iwashina and A. Kudo, Facile fabrication of an efficient BiVO4 thin film electrode for water splitting under visible light irradiation, *Proc. Natl. Acad. Sci. U. S. A.*, 2012, **109**(29), 11564–11569.
63 G. Hodes, D. Cahen and J. Manassen, Tungsten trioxide as a photoanode for a photoelectrochemical cell (PEC), *Nature*, 1976, **260**(5549), 312–313.
64 J. A. Seabold, K. Zhu and N. R. Neale, Efficient solar photoelectrolysis by nanoporous Mo: BiVO 4 through controlled electron transport, *Phys. Chem. Chem. Phys.*, 2014, **16**(3), 1121–1131.
65 S. Hoang, S. P. Berglund, N. T. Hahn, A. J. Bard and C. Buddie Mullins, Enhancing visible light photo-oxidation of water with TiO_2 nanowire arrays via cotreatment with H_2 and NH_3: synergistic effects between Ti^{3+} and N, *J. Am. Chem. Soc.*, 2012, **134**(8), 3659–3662.
66 T. Hisatomi and F. Le, Formal, M. Cornuz, J. Brillet, N. Tétreault, K. Sivula, and M. Grätzel. Cathodic shift in onset potential of solar oxygen evolution on hematite by 13-group oxide overlayers, *Energy Environ. Sci.*, 2011, **4**(7), 2512–2515.
67 A. J. Bard, Photoelectrochemistry and heterogeneous photo-catalysis at semiconductors, *J. Photochem.*, 1979, **10**(1), 59–75.
68 A. Thakur, D. Ghosh, P. Devi, K.-H. Kim and P. Kumar, Current progress and challenges in photoelectrode materials for the production of hydrogen, *Chem. Eng. J.*, 2020, **397**, 125415.
69 Q. Chen, G. Fan, H. Fu, Z. Li and Z. Zou, Tandem photoelectrochemical cells for solar water splitting, *Adv. Phys.: X*, 2018, **3**(1), 1487267.
70 O. Khaselev and J. A. Turner, A monolithic photovoltaic-photoelectrochemical device for hydrogen production via water splitting, *Science*, 1998, **280**(5362), 425–427.
71 Y. Zheng, L. Lin, B. Wang and X. Wang, Graphitic carbon nitride polymers toward sustainable photoredox catalysis, *Angew. Chem., Int. Ed.*, 2015, **54**(44), 12868–12884.
72 M. Huang, Y.-L. Zhao, W. Xiong, S. V. Kershaw, Y. Yu, W. Li, T. Dudka and R.-Q. Zhang, Collaborative enhancement of photon harvesting and charge carrier dynamics in carbon nitride photoelectrode, *Appl. Catal., B*, 2018, **237**, 783–790.
73 J. Xu, S. Cao, T. Brenner, X. Yang, J. Yu, M. Antonietti and M. Shalom, Supramolecular chemistry in molten sulfur: preorganization effects leading to marked enhancement of carbon nitride photoelectrochemistry, *Adv. Funct. Mater.*, 2015, **25**(39), 6265–6271.
74 F. Qi, Y. Li, Y. Wang, Y. Wang, S. Liu and X. Zhao, Ag-Doped g-C_3N_4 film electrode: fabrication, characterization and photoelectrocatalysis property, *RSC Adv.*, 2016, **6**(84), 81378–81385.
75 W. Zhang, J. Albero, L. Xi, K. M. Lange, H. Garcia, X. Wang and M. Shalom, One-pot synthesis of nickel-modified carbon nitride layers toward efficient photoelectrochemical cells, *ACS Appl. Mater. Interfaces*, 2017, **9**(38), 32667–32677.
76 J. Jing, Z. Chen and C. Feng, Dramatically enhanced photoelectrochemical properties and transformed p/n type of g-C_3N_4 caused by K and I co-doping, *Electrochim. Acta*, 2019, **297**, 488–496.
77 X. She, L. Liu, H. Ji, Z. Mo, Y. Li, L. Huang, D. Du, H. Xu and H. Li, Template-free synthesis of 2D porous ultrathin nonmetal-doped g-C_3N_4 nanosheets with highly efficient photocatalytic H_2 evolution from water under visible light, *Appl. Catal., B*, 2016, **187**, 144–153.
78 Z. Wang, X. Hu, G. Zou, Z. Huang, Z. Tang, Q. Liu, G. Hu and D. Geng, Advances in constructing polymeric carbon-nitride-based nanocomposites and their applications in energy chemistry, *Sustainable Energy Fuels*, 2019, **3**(3), 611–655.

79 F. K. Kessler, Y. Zheng, D. Schwarz, C. Merschjann, W. Schnick, X. Wang and M. J. Bojdys, Functional carbon nitride materials—design strategies for electrochemical devices. Nature Reviews, *Materials*, 2017, **2**(6), 1–17.

80 Y. Li, M. Zhou, B. Cheng and Y. Shao, Recent advances in g-C_3N_4-based heterojunction photocatalysts, *J. Mater. Sci. Technol.*, 2020, **56**, 1–17.

81 C.-H. Wang, D.-D. Qin, D.-L. Shan, J. Gu, Y. Yan, J. Chen and Q.-H. Wang, *et al.*, Assembly of g-C_3N_4-based type II and Z-scheme heterojunction anodes with improved charge separation for photoelectrojunction water oxidation, *Phys. Chem. Chem. Phys.*, 2017, **19**(6), 4507–4515.

82 G. K. Mor, O. K. Varghese, M. Paulose, K. Shankar and C. A. Grimes, A review on highly ordered, vertically oriented TiO_2 nanotube arrays: Fabrication, material properties, and solar energy applications, *Sol. Energy Mater. Sol. Cells*, 2006, **90**(14), 2011–2075.

83 G. Wang, Y. Ling, H. Wang, L. Xihong and Y. Li, Chemically modified nanostructures for photoelectrochemical water splitting, *J. Photochem. Photobiol., C*, 2014, **19**, 35–51.

84 B. Babu, J. Shim and K. Yoo, Efficient solar-light-driven photoelectrochemical water oxidation of one-step in-situ synthesized Co-doped g-C_3N_4 nanolayers, *Ceram. Int.*, 2020, **46**(10), 16422–16430.

85 A. E. A. Aboubakr, W. M. A. El Rouby, M. D. Khan, A. A. Farghali and N. Revaprasadu, ZnCr-CO_3 LDH/ruptured tubular g-C_3N_4 composite with increased specific surface area for enhanced photoelectrochemical water splitting, *Appl. Surf. Sci.*, 2020, **508**, 145100.

86 P. Han, W. Martens, E. R. Waclawik, S. Sarina and H. Zhu, Metal nanoparticle photocatalysts: synthesis, characterization, and application, *Part. Part. Syst. Charact.*, 2018, **35**(6), 1700489.

87 G. Liu, K. Du, J. Xu, G. Chen, M. Gu, C. Yang, K. Wang and H. Jakobsen, Plasmon-dominated photoelectrodes for solar water splitting, *J. Mater. Chem. A*, 2017, **5**(9), 4233–4253.

88 A. Eftekhari, V. J. Babu and S. Ramakrishna, Photoelectrode nanomaterials for photoelectrochemical water splitting, *Int. J. Hydrogen Energy*, 2017, **42**(16), 11078–11109.

89 F. Dong, Z. Zhao, Y. Sun, Y. Zhang, S. Yan and Z. Wu, An advanced semimetal–organic Bi spheres–g-C_3N_4 nanohybrid with SPR-enhanced visible-light photocatalytic performance for NO purification, *Environ. Sci. Technol.*, 2015, **49**(20), 12432–12440.

90 X. Fang, Y. Tang, Y.-J. Ma, G. Xiao, P. Li and D. Yan, Ultralong-lived triplet excitons of room-temperature phosphorescent carbon dots located on g-C3N4 to boost photocatalysis, *Sci. China Mater.*, 2023, **66**(2), 664–671.

91 P. Li, Y. Lin, Z. Qi and D. Yan, Efficient photoelectrocatalytic CO 2 reduction to CH 3 OH via porous gC 3 N 4 nanosheets modified with cobalt phthalocyanine in ionic liquids, *J. Mater. Chem. A*, 2023, **11**(39), 21078–21088.

92 M. Joseph, N. K. Mohammed Sadik, S. N. Remello, S. Haridas and S. De, Through Space Sigma Donation π Acceptor Assisted Photocatalytic Degradation of Ciprofloxacin on TCPP Supported g-C3N4, *ChemistrySelect*, 2023, **8**(7), e202203348.

93 S. Lou, Z. Zhou, Y. Shen, Z. Zhan, J. Wang, S. Liu and Y. Zhang, Comparison study of the photoelectrochemical activity of carbon nitride with different photoelectrode configurations, *ACS Appl. Mater. Interfaces*, 2016, **8**(34), 22287–22294.

94 W. M. A. El Rouby, A. E. A. Aboubakr, M. D. Khan, A. A. Farghali, P. Millet and N. Revaprasadu, Synthesis and characterization of Bi-doped g-C_3N_4 for photoelectrochemical water oxidation, *Sol. Energy*, 2020, **211**, 478–487.

95 Y. Du, R. Ma, L. Wang, J. Qian and Q. Wang, 2D/1D BiOI/g-C_3N_4 nanotubes heterostructure for photoelectrochemical overall water splitting, *Sci. Total Environ.*, 2022, **838**, 156166.

96 A. E. A. Bakr, W. M. A. El Rouby, M. D. Khan, A. A. Farghali, B. Xulu and N. Revaprasadu, Synthesis and characterization of Z-scheme α-Fe_2O_3 NTs/ruptured tubular g-C3N4 for enhanced photoelectrochemical water oxidation, *Sol. Energy*, 2019, **193**, 403–412.

97 T. Song, X. Zhang and P. Yang, Bifunctional Nitrogen-Doped Carbon Dots in g-C_3N_4/WO_x Heterojunction for Enhanced Photocatalytic Water-Splitting Performance, *Langmuir*, 2021, **37**(14), 4236–4247.

98 K. M. Alam, P. Kumar, P. Kar, U. K. Thakur, S. Zeng, K. Cui and K. Shankar, Enhanced charge separation in g-C_3N_4–BiOI heterostructures for visible light driven photoelectrochemical water splitting, *Nanoscale Adv.*, 2019, **1**(4), 1460–1471.

99 P. Wen, Y. Sun, H. Li, Z. Liang, H. Wu, J. Zhang, H. Zeng, S. M. Geyer and L. Jiang, A highly active three-dimensional Z-scheme ZnO/Au/g-C_3N_4 photocathode for efficient photoelectrochemical water splitting, *Appl. Catal., B*, 2020, **263**, 118180.

100 Y. Fang, Y. Xu, X. Li, Y. Ma and X. Wang, Coating polymeric carbon nitride photoanodes on conductive Y: ZnO nanorod arrays for overall water splitting, *Angew. Chem.*, 2018, **130**(31), 9897–9901.

101 J. Safaei, N. A. Mohamed, M. F. Mohamad Noh, M. F. Soh, M. A. Riza, N. S. Mohamed Mustakim, N. A. Ludin, M. A. Ibrahim, W. N. R. W. Isahak and M. A. Mat Teridi, Facile fabrication of graphitic carbon nitride,(g-C_3N_4) thin film, *J. Alloys Compd.*, 2018, **769**, 130–135.

102 K. Li, X. Zeng, S. Gao, L. Ma, Q. Wang, H. Xu, Z. Wang, B. Huang, Y. Dai and J. Lu, Ultrasonic-assisted pyrolyzation fabrication of reduced SnO_{2-x}/g-C_3N_4 heterojunctions: Enhance photoelectrochemical and photocatalytic activity under visible LED light irradiation, *Nano Res.*, 2016, **9**, 1969–1982.

103 K. Li, Z. Huang, X. Zeng, B. Huang, S. Gao and J. Lu, Synergetic effect of Ti^{3+} and oxygen doping on enhancing photoelectrochemical and photocatalytic properties of TiO_2/g-C_3N_4 heterojunctions, *ACS Appl. Mater. Interfaces*, 2017, **9**(13), 11577–11586.

104 Y. Liu, F. Y. Su, Y. X. Yu and W. D. Zhang, Nano g-C_3N_4 modified Ti-Fe_2O_3 vertically arrays for efficient photoelectrochemical generation of hydrogen under visible light, *Int. J. Hydrogen Energy*, 2016, **41**(18), 7270–7279.

105 J. Safaei, H. Ullah, N. A. Mohamed, M. F. Mohamad Noh, M. F. Soh, A. A. Tahir, N. A. Ludin, M. A. Ibrahim,

W. N. R. W. Isahak and M. A. Mat Teridi, Enhanced photoelectrochemical performance of Z-scheme g-C3N4/BiVO4 photocatalyst, *Appl. Catal., B*, 2018, **234**, 296–310.

106 F. Liang and Y. Zhu, Enhancement of mineralization ability for phenol via synergetic effect of photoelectrocatalysis of g-C_3N_4 film, *Appl. Catal., B*, 2016, **180**, 324–329.

107 L. Liu, M. Wang and C. Wang, In-situ synthesis of graphitic carbon nitride/iron oxide– copper composites and their application in the electrochemical detection of glucose, *Electrochim. Acta*, 2018, **265**, 275–283.

108 H. Miao, G. Zhang, X. Hu, J. Mu, T. Han, J. Fan, C. Zhu, L. Song, J. Bai and X. Hou, A novel strategy to prepare 2D g-C_3N_4 nanosheets and their photoelectrochemical properties, *J. Alloys Compd.*, 2017, **690**, 669–676.

109 J. Duan, S. Chen, M. Jaroniec and S. Z. Qiao, Porous C_3N_4 nanolayers@ N-graphene films as catalyst electrodes for highly efficient hydrogen evolution, *ACS Nano*, 2015, **9**(1), 931–940.

110 X. Zhang, X. Xie, H. Wang, J. Zhang, B. Pan and Y. Xie, Enhanced photoresponsive ultrathin graphitic-phase C_3N_4 nanosheets for bioimaging, *J. Am. Chem. Soc.*, 2013, **135**(1), 18–21.

111 K. G. Zhou, D. McManus, E. Prestat, X. Zhong, Y. Shin, H. L. Zhang, S. J. Haigh and C. Casiraghi, Self-catalytic membrane photo-reactor made of carbon nitride nanosheets, *J. Mater. Chem. A*, 2016, **4**(30), 11666–11671.

112 E. J. Son, S. H. Lee, S. K. Kuk, M. Pesic, D. S. Choi, J. W. Ko, K. Kim, F. Hollmann and C. B. Park, Carbon Nanotube–Graphitic Carbon Nitride Hybrid Films for Flavoenzyme-Catalyzed Photoelectrochemical Cells, *Adv. Funct. Mater.*, 2018, **28**(24), 1705232.

113 Y. Wang, X. Zhao, Y. Tian, Y. Wang, A. K. Jan and Y. Chen, Facile Electrospinning Synthesis of Carbonized Polyvinylpyrrolidone (PVP)/g-C3N4 Hybrid Films for Photoelectrochemical Applications, *Chem. – Eur. J.*, 2017, **23**(2), 419–426.

114 Y. Wang, J. Sun, J. Li and X. Zhao, Electrospinning preparation of nanostructured g-C_3N_4/$BiVO_4$ composite films with an enhanced photoelectrochemical performance, *Langmuir*, 2017, **33**(19), 4694–4701.

115 C. He, J. H. Zhang, W. X. Zhang and T. T. Li, Type-II InSe/g-C_3N_4 heterostructure as a high-efficiency oxygen evolution reaction catalyst for photoelectrochemical water splitting, *J. Phys. Chem. Lett.*, 2019, **10**(11), 3122–3128.

116 G. Peng, M. Volokh, J. Tzadikov, J. Sun and M. Shalom, . Carbon nitride/reduced graphene oxide film with enhanced electron diffusion length: an efficient photoelectrochemical cell for hydrogen generation, *Adv. Energy Mater.*, 2018, **8**(23), 1800566.

117 C. H. Choi, L. Lin, S. Gim, S. Lee, H. Kim, X. Wang and W. Choi, Polymeric carbon nitride with localized aluminum coordination sites as a durable and efficient photocatalyst for visible light utilization, *ACS Catal.*, 2018, **8**(5), 4241–4256.

118 H. Bae, V. Burungale, W. Na, H. Rho, S. H. Kang, S. W. Ryu and J. S. Ha, Nanostructured CuO with a thin g-C_3N_4 layer as a highly efficient photocathode for solar water splitting, *RSC Adv.*, 2021, **11**(26), 16083–16089.

119 J. Xu and M. Shalom, . Electrophoretic deposition of carbon nitride layers for photoelectrochemical applications, *ACS Appl. Mater. Interfaces*, 2016, **8**(20), 13058–13063.

120 M. Basu, Z. W. Zhang, C. J. Chen, T. H. Lu, S. F. Hu and R. S. Liu, $CoSe_2$ embedded in C_3N_4: An efficient photocathode for photoelectrochemical water splitting, *ACS Appl. Mater. Interfaces*, 2016, **8**(40), 26690–26696.

121 S. Samanta, S. Martha and K. Parida, Facile synthesis of Au/g-C_3N_4 nanocomposites: an inorganic/organic hybrid plasmonic photocatalyst with enhanced hydrogen gas evolution under visible-light irradiation, *ChemCatChem*, 2014, **6**(5), 1453–1462.

122 C. Li, C. B. Cao and H. S. Zhu, Graphitic carbon nitride thin films deposited by electrodeposition, *Mater. Lett.*, 2004, **58**(12–13), 1903–1906.

123 D. Kang, T. W. Kim, S. R. Kubota, A. C. Cardiel, H. G. Cha and K. S. Choi, Electrochemical synthesis of photoelectrodes and catalysts for use in solar water splitting, *Chem. Rev.*, 2015, **115**(23), 12839–12887.

124 S. Zhang, J. Yan, S. Yang, Y. Xu, X. Cai, X. Li, X. Zhang, F. Peng and Y. Fang, Electrodeposition of Cu_2O/g-C_3N_4 heterojunction film on an FTO substrate for enhancing visible light photoelectrochemical water splitting, *Chin. J. Catal.*, 2017, **38**(2), 365–371.

125 H. Qi, B. Sun, J. Dong, L. Cui, T. Feng and S. Ai, Facile synthesis of two-dimensional tailored graphitic carbon nitride with enhanced photoelectrochemical properties through a three-step polycondensation method for photocatalysis and photoelectrochemical immunosensor, *Sens. Actuators, B*, 2019, **285**, 42–48.

126 D. B. Velusamy, M. A. Haque, M. R. Parida, F. Zhang, T. Wu, O. F. Mohammed and H. N. Alshareef, 2D organic–inorganic hybrid thin films for flexible UV–visible photodetectors, *Adv. Funct. Mater.*, 2017, **27**(15), 1605554.

127 L. Jia, H. Wang, D. Dhawale, C. Anand, M. A. Wahab, Q. Ji, K. Ariga and A. Vinu, Highly ordered macro-mesoporous carbon nitride film for selective detection of acidic/basic molecules, *Chem. Commun.*, 2014, **50**(45), 5976–5979.

128 H. Huang, R. Chen, J. Ma, L. Yan, Y. Zhao, Y. Wang, W. Zhang, J. Fan and X. Chen, Graphitic carbon nitride solid nanofilms for selective and recyclable sensing of Cu^{2+} and Ag^{+} in water and serum, *Chem. Commun.*, 2014, **50**(97), 15415–15418.

129 J. Bian, Q. Li, C. Huang, J. Li, Y. Guo, M. Zaw and R. Q. Zhang, Thermal vapor condensation of uniform graphitic carbon nitride films with remarkable photocurrent density for photoelectrochemical applications, *Nano Energy*, 2015, **15**, 353–361.

130 X. Lv, M. Cao, W. Shi, M. Wang and Y. Shen, A new strategy of preparing uniform graphitic carbon nitride films for photoelectrochemical application, *Carbon*, 2017, **117**, 343–350.

131 J. Bian, L. Xi, C. Huang, K. M. Lange, R.-Q. Zhang and M. Shalom, . Efficiency enhancement of carbon nitride

photoelectrochemical cells via tailored monomers design, *Adv. Energy Mater.*, 2016, **6**(12), 1600263.

132 J. Bian, L. Xi, J. Li, Z. Xiong, C. Huang, K. M. Lange, J. Tang, M. Shalom and R.-Q. Zhang, C═C π bond modified graphitic carbon nitride films for enhanced photoelectrochemical cell performance, *Chem. – Asian J.*, 2017, **12**(9), 1005–1012.

133 X. Lu, Z. Liu, J. Li, J. Zhang and Z. Guo, Novel framework g-C_3N_4 film as efficient photoanode for photoelectrochemical water splitting, *Appl. Catal., B*, 2017, **209**, 657–662.

134 J. Xu, I. Herraiz-Cardona, X. Yang, S. Gimenez, M. Antonietti and M. Shalom, . The complex role of carbon nitride as a sensitizer in photoelectrochemical cells, *Adv. Opt. Mater.*, 2015, **3**(8), 1052–1058.

135 J. Bian, J. Li, S. Kalytchuk, Y. Wang, Q. Li, T. C. Lau, T. A. Niehaus, A. L. Rogach and R.-Q. Zhang, Efficient emission facilitated by multiple energy level transitions in uniform graphitic carbon nitride films deposited by thermal vapor condensation, *ChemPhysChem*, 2015, **16**(5), 954–959.

136 Q. Guo, L. Fu, T. Yan, W. Tian, D. Ma, J. Li, Y. Jiang and X. Wang, Improved photocatalytic activity of porous ZnO nanosheets by thermal deposition graphene-like g-C3N4 for CO2 reduction with H2O vapor, *Appl. Surf. Sci.*, 2020, **509**, 144773.

137 Q. Ruan, W. Luo, J. Xie, Y. Wang, X. Liu, Z. Bai, C. J. Carmalt and J. Tang, A nanojunction polymer photoelectrode for efficient charge transport and separation, *Angew. Chem., Int. Ed.*, 2017, **56**(28), 8221–8225.

138 J. Bian, C. Huang and R.-Q. Zhang, Graphitic carbon nitride film: an emerging star for catalytic and optoelectronic applications, *ChemSusChem*, 2016, **9**(19), 2723–2735.

139 M. Shalom, S. Gimenez, F. Schipper, I. Herraiz-Cardona, J. Bisquert and M. Antonietti, Controlled carbon nitride growth on surfaces for hydrogen evolution electrodes, *Angew. Chem.*, 2014, **126**(14), 3728–3732.

140 L. Ye and S. Chen, Fabrication and high visible-light-driven photocurrent response of g-C_3N_4 film: the role of thiourea, *Appl. Surf. Sci.*, 2016, **389**, 1076–1083.

141 Y.-S. Jun, E. Z. Lee, X. Wang, W. H. Hong, G. D. Stucky and A. Thomas, From melamine-cyanuric acid supramolecular aggregates to carbon nitride hollow spheres, *Adv. Funct. Mater.*, 2013, **23**(29), 3661–3667.

142 J. Xu, T. J. K. Brenner, L. Chabanne, D. Neher, M. Antonietti and M. Shalom., Liquid-based growth of polymeric carbon nitride layers and their use in a mesostructured polymer solar cell with V oc exceeding 1 V, *J. Am. Chem. Soc.*, 2014, **136**(39), 13486–13489.

143 R. Cazelles, J. Liu and M. Antonietti, Hybrid C_3N_4/Fluorine-Doped Tin Oxide Electrode Transfers Hydride for 1, 4-NADH Cofactor Regeneration, *ChemElectroChem*, 2015, **2**(3), 333–337.

144 J. Liu, H. Wang, Z. P. Chen, H. Moehwald, S. Fiechter, R. van de Krol, L. Wen, L. Jiang and M. Antonietti, Microcontact-printing-assisted access of graphitic carbon nitride films with favorable textures toward photoelectrochemical application, *Adv. Mater.*, 2015, **27**(4), 712–718.

145 X. Xie, X. Fan, X. Huang, T. Wang and J. He, *In situ* growth of graphitic carbon nitride films on transparent conducting substrates via a solvothermal route for photoelectrochemical performance, *RSC Adv.*, 2016, **6**(12), 9916–9922.

146 Q. Gu, X. Gong, Q. Jia, J. Liu, Z. Gao, X. Wang, J. Long and C. Xue, Compact carbon nitride based copolymer films with controllable thickness for photoelectrochemical water splitting, *J. Mater. Chem. A*, 2017, **5**(36), 19062–19071.

147 X. Bai, L. Wang, R. Zong and Y. Zhu, Photocatalytic activity enhanced via g-C_3N_4 nanoplates to nanorods, *J. Phys. Chem. C*, 2013, **117**(19), 9952–9961.

148 A. Mehtab, S. M. Alshehri and T. Ahmad, Photocatalytic and photoelectrocatalytic water splitting by porous g-C_3N_4 nanosheets for hydrogen generation, *ACS Appl. Nano Mater.*, 2022, **5**(9), 12656–12665.

149 Y. Zhang, A. Thomas, M. Antonietti and X. Wang, Activation of carbon nitride solids by protonation: morphology changes, enhanced ionic conductivity, and photoconduction experiments, *J. Am. Chem. Soc.*, 2009, **131**(1), 50–51.

150 Y. Bu, Z. Chen, T. Xie, W. Li and J. P. Ao, Fabrication of C_3N_4 ultrathin flakes by mechanical grind method with enhanced photocatalysis and photoelectrochemical performance, *RSC Adv.*, 2016, **6**(53), 47813–47819.

151 G. Peng, J. Albero, H. Garcia and M. Shalom, . A water-splitting carbon nitride photoelectrochemical cell with efficient charge separation and remarkably low onset potential, *Angew. Chem., Int. Ed.*, 2018, **57**(48), 15807–15811.

152 N. A. Mohamed, J. Safaei, A. F. Ismail, M. F. Mohamad Noh, N. A. Arzaee, N. N. Mansor, M. A. Ibrahim, N. A. Ludin, J. S. Sagu and M. A. Mat Teridi, Fabrication of exfoliated graphitic carbon nitride,(g-C_3N_4) thin film by methanolic dispersion, *J. Alloys Compd.*, 2020, **818**, 152916.

153 J. Qin, J. Barrio, G. Peng, J. Tzadikov, L. Abisdris, M. Volokh and M. Shalom, . Direct growth of uniform carbon nitride layers with extended optical absorption towards efficient water-splitting photoanodes, *Nat. Commun.*, 2020, **11**(1), 4701.

154 B. Guo, L. Tian, W. Xie, A. Batool, G. Xie, Q. Xiang, S. U. Jan, R. Boddula and J. R. Gong, Vertically aligned porous organic semiconductor nanorod array photoanodes for efficient charge utilization, *Nano Lett.*, 2018, **18**(9), 5954–5960.

155 Y. Fang, X. Li and X. Wang, Synthesis of polymeric carbon nitride films with adhesive interfaces for solar water splitting devices, *ACS Catal.*, 2018, **8**(9), 8774–8780.

156 Y. Fang, X. Li, Y. Wang, C. Giordano and X. Wang, Gradient sulfur doping along polymeric carbon nitride films as visible light photoanodes for the enhanced water oxidation, *Appl. Catal., B*, 2020, **268**, 118398.

157 A. E. A. Aboubakr, W. M. A. El Rouby, M. D. Khan, N. Revaprasadu and P. Millet, Effect of morphology and non-metal doping (P and S) on the activity of graphitic carbon nitride toward photoelectrochemical water oxidation, *Sol. Energy Mater. Sol. Cells*, 2021, **232**, 111326.

158 S. Vinoth, W. J. Ong and A. Pandikumar, Sulfur-doped graphitic carbon nitride incorporated bismuth oxychloride/

Cobalt based type-II heterojunction as a highly stable material for photoelectrochemical water splitting, *J. Colloid Interface Sci.*, 2021, **591**, 85–95.

159 J. Su, P. Geng, X. Li, Q. Zhao, X. Quan and G. Chen, Novel phosphorus doped carbon nitride modified TiO_2 nanotube arrays with improved photoelectrochemical performance, *Nanoscale*, 2015, **7**(39), 16282–16289.

160 W. Kong, X. Zhang, B. Chang, Y. Zhou, S. Zhang, G. He, B. Yang and J. Li, Fabrication of B doped g-C_3N_4/TiO_2 heterojunction for efficient photoelectrochemical water oxidation, *Electrochim. Acta*, 2018, **282**, 767–774.

161 N. Lei, J. Li, Q. Song and Z. Liang, Construction of g-C_3N_4/BCN two-dimensional heterojunction photoanode for enhanced photoelectrochemical water splitting, *Int. J. Hydrogen Energy*, 2019, **44**(21), 10498–10507.

162 J. Qin, Y. Jiao, M. Liu, Y. Li and J. Wang, Heat treatment to prepare boron doped g-C_3N_4 nanodots/carbon-rich g-C_3N_4 nanosheets heterojunction with enhanced photocatalytic performance for water splitting hydrogen evolution, *J. Alloys Compd.*, 2022, **898**, 162846.

163 S. Vinoth and A. Pandikumar, Ni integrated S-gC_3N_4/BiOBr based Type-II heterojunction as a durable catalyst for photoelectrochemical water splitting, *Renewable Energy*, 2021, **173**, 507–519.

164 P. Chaudhary and P. P. Ingole, Nickel incorporated graphitic carbon nitride supported copper sulfide for efficient noble-metal-free photo-electrochemical water splitting, *Electrochim. Acta*, 2020, **357**, 136798.

165 K. N. Mahdi and E. K. Goharshadi, Decoration of graphene oxide as a cocatalyst on Bi doped g-C_3N_4 photoanode for efficient solar water splitting, *J. Electroanal. Chem.*, 2022, **904**, 115933.

166 F. Wu, Y. Ma and Y. H. Hu, Near infrared light-driven photoelectrocatalytic water splitting over P-doped g-C_3N_4. ACS Applied Energy, *Materials*, 2020, **3**(11), 11223–11230.

167 I. N. Reddy, L. V. Reddy, N. Jayashree, C. V. Reddy, M. Cho, D. Kim and J. Shim, Vanadium-doped graphitic carbon nitride for multifunctional applications: Photoelectrochemical water splitting and antibacterial activities, *Chemosphere*, 2021, **264**, 128593.

168 Y. Li, *et al.*, Composite of Cobalt-C_3N_4 on TiO_2 Nanorod Arrays as Co-catalyst for Enhanced Photoelectrochemical Water Splitting, *ChemistrySelect*, 2021, **6**(17), 4319–4329.

169 K. N. Mahdi, E. K. Goharshadi and S. J. Mahdizadeh, Efficient photoelectrocatalytic water oxidation by palladium doped g-C_3N_4 electrodeposited thin film, *J. Phys. Chem. C*, 2019, **123**(43), 26106–26115.

170 S. Zhao, Y. Zhang, Y. Wang, Y. Zhou, K. Qiu, C. Zhang, J. Fang and X. Sheng, Ionic liquid-assisted synthesis of Br-modified g-C_3N_4 semiconductors with high surface area and highly porous structure for photoredox water splitting, *J. Power Sources*, 2017, **370**, 106–113.

171 D. R. Paul, R. Sharma, S. Singh, P. Singh, P. Panchal, A. Sharma, P. Devi and S. P. Nehra, Mg/Li Co-doped g-C_3N_4: An excellent photocatalyst for wastewater remediation and hydrogen production applications towards sustainable development, *Int. J. Hydrogen Energy*, 2023, **48**(96), 37746–37761.

172 P. Trogadas, T. F. Fuller and P. Strasser, Carbon as catalyst and support for electrochemical energy conversion, *Carbon*, 2014, **75**, 5–42.

173 X. Zhao, D. Pan, X. Chen, R. Li, T. Jiang, W. Wang, G. Li and D. Y. C. Leung, g-C_3N_4 photoanode for photoelectrocatalytic synergistic pollutant degradation and hydrogen evolution, *Appl. Surf. Sci.*, 2019, **467**, 658–665.

174 S. Yousefzadeh and B. Fathi, Construction of carbon nanotube-g-C_3N_4 nanocomposite photoanode for the enhanced photoelectrochemical activity in water splitting, *J. Electroanal. Chem.*, 2020, **878**, 114580.

175 Y. Wei, Z. Wang, J. Su and L. Guo, Metal-Free Flexible Protonated g-C_3N_4/Carbon Dots Photoanode for Photoelectrochemical Water Splitting, *ChemElectroChem*, 2018, **5**(19), 2734–2737.

176 S. S. M. Bhat, S. E. Jun, S. A. Lee, T. H. Lee and H. W. Jang, Influence of C_3N_4 precursors on photoelectrochemical behavior of TiO_2/C_3N_4 photoanode for solar water oxidation, *Energies*, 2020, **13**(4), 974.

177 K. Shankar, J. I. Basham, N. K. Allam, O. K. Varghese, G. K. Mor, X. Feng, M. Paulose, J. A. Seabold, K. S. Choi and C. A. Grimes, Recent advances in the use of TiO_2 nanotube and nanowire arrays for oxidative photoelectrochemistry, *J. Phys. Chem. C*, 2009, **113**(16), 6327–6359.

178 A. Zhang, M. Zhou, L. Han and Q. Zhou, Combined potential of three catalysis types on TiO_2 nanotube (TNT)/Ti and nanoparticle (TNP)/Ti photoelectrodes: A comparative study, *Appl. Catal., A*, 2010, **385**(1–2), 114–122.

179 X. Zhou, B. Jin, L. Li, F. Peng, H. Wang, H. Yu and Y. Fang, A carbon nitride/TiO_2 nanotube array heterojunction visible-light photocatalyst: synthesis, characterization, and photoelectrochemical properties, *J. Mater. Chem.*, 2012, **22**(34), 17900–17905.

180 M. Yang, J. Liu, X. Zhang, S. Qiao, H. Huang, Y. Liu and Z. Kang, C_3N_4-sensitized TiO_2 nanotube arrays with enhanced visible-light photoelectrochemical performance, *Phys. Chem. Chem. Phys.*, 2015, **17**(27), 17887–17893.

181 L. Wang, W. Si, Y. Ye, S. Wang, F. Hou, X. Hou, H. Cai, S. X. Dou and J. Liang, Cu-ion-implanted and polymeric carbon nitride-decorated TiO_2 nanotube array for unassisted photoelectrochemical water splitting, *ACS Appl. Mater. Interfaces*, 2021, **13**(37), 44184–44194.

182 F. Zhang, J. Liu, H. Yue, G. Cheng and X. Xue, Construction of g-C_3N_4 nanoparticles modified TiO_2 nanotube arrays with Z-scheme heterojunction for enhanced photoelectrochemical properties, *J. Mater. Sci.*, 2023, 1–13.

183 M. Sun, Y. Fang, Y. Kong, S. Sun, Z. Yu and A. Umar, Graphitic carbon nitride (g-C_3N_4) coated titanium oxide nanotube arrays with enhanced photo-electrochemical performance, *Dalton Trans.*, 2016, **45**(32), 12702–12709.

184 C. Liu, F. Wang, J. Zhang, K. Wang, Y. Qiu, Q. Liang and Z. Chen, Efficient photoelectrochemical water splitting by g-C_3N_4/TiO_2 nanotube array heterostructures, *Nano-Micro Lett.*, 2018, **10**, 1–13.

185 X. Fan, T. Wang, B. Gao, H. Gong, H. Xue, H. Guo, L. Song, W. Xia, X. Huang and J. He, Preparation of the TiO_2/

graphic carbon nitride core–shell array as a photoanode for efficient photoelectrochemical water splitting, *Langmuir*, 2016, **32**(50), 13322–13332.

186 C. Murugan, K. B. Bhojanaa, W. J. Ong, K. Jothivenkatachalam and A. Pandikumar, Improving hole mobility with the heterojunction of graphitic carbon nitride and titanium dioxide via soft template process in photoelectrocatalytic water splitting, *Int. J. Hydrogen Energy*, 2019, **44**(59), 30885–30898.

187 F. Qi, W. An, H. Wang, J. Hu, H. Guo, L. Liu and W. Cui, Combing oxygen vacancies on TiO_2 nanorod arrays with g-C_3N_4 nanosheets for enhancing photoelectrochemical degradation of phenol, *Mater. Sci. Semicond. Process.*, 2020, **109**, 104954.

188 L. Xiao, T. Liu, M. Zhang, Q. Li and J. Yang, Interfacial construction of zero-dimensional/one-dimensional g-C_3N_4 nanoparticles/TiO_2 nanotube arrays with Z-scheme heterostructure for improved photoelectrochemical water splitting, *ACS Sustainable Chem. Eng.*, 2018, **7**(2), 2483–2491.

189 J. Su, L. Zhu and G. Chen, Ultrasmall graphitic carbon nitride quantum dots decorated self-organized TiO_2 nanotube arrays with highly efficient photoelectrochemical activity, *Appl. Catal., B*, 2016, **186**, 127–135.

190 B. Sun, N. Lu, Y. Su, H. Yu, X. Meng and Z. Gao, Decoration of TiO_2 nanotube arrays by graphitic-C_3N_4 quantum dots with improved photoelectrocatalytic performance, *Appl. Surf. Sci.*, 2017, **394**, 479–487.

191 L. Huang, Q. Meng, C. Shang, M. Jin, L. Shui, Y. Zhang and Z. Zhang, *et al.*, Modified nanopillar arrays for highly stable and efficient photoelectrochemical water splitting, *Global Challenges*, 2019, **3**(3), 1800027.

192 Y. Wang, Y. Zhang, M. Di, L. Fu, H. Pan, K. Zhang and Y. Xu, *et al.*, Realization of ultrathin red 2D carbon nitride sheets to significantly boost the photoelectrochemical water splitting performance of TiO_2 photoanodes, *Chem. Eng. J.*, 2020, **396**, 125267.

193 P. Mary Rajaitha, K. Shamsa, C. Murugan, K. B. Bhojanaa, S. Ravichandran, K. Jothivenkatachalam and A. Pandikumar, Graphitic carbon nitride nanoplatelets incorporated titania based type-II heterostructure and its enhanced performance in photoelectrocatalytic water splitting, *SN Appl. Sci.*, 2020, **2**, 1–14.

194 K. Huang, C. Li, X. Zhang, X. Meng, L. Wang, W. Wang and Z. Li, TiO_2 nanorod arrays decorated by nitrogen-doped carbon and g-C3N4 with enhanced photoelectrocatalytic activity, *Appl. Surf. Sci.*, 2020, **518**, 146219.

195 T. T. Nguyen, H. H. Tran, T. M. Cao and V. V. Pham, Direct fabrication of graphitic carbon nitride-wrapped titanate nanotube arrays toward photoelectrochemical water oxidation in neutral medium, *Korean J. Chem. Eng.*, 2022, **39**(9), 2523–2531.

196 Y. Liu, P. Wang, C. Wang and Y. Ao, Polymeric carbon nitride coated Nb-TiO_2 nanorod arrays with enhanced photoelectrocatalytic activity under visible light irradiation, *Inorg. Chem. Commun.*, 2019, **101**, 113–116.

197 Y. Ding, S. Maitra, C. Wang, R. Zheng, M. Zhang, T. Barakat and S. Roy, *et al.*, Hydrophilic bi-functional B-doped g-C_3N_4 hierarchical architecture for excellent photocatalytic H_2O_2 production and photoelectrochemical water splitting, *J. Energy Chem.*, 2022, **70**, 236–247.

198 P. Kumar, U. K. Thakur, K. Alam, P. Kar, R. Kisslinger, S. Zeng, S. Patel and K. Shankar, Arrays of TiO_2 nanorods embedded with fluorine doped carbon nitride quantum dots (CNFQDs) for visible light driven water splitting, *Carbon*, 2018, **137**, 174–187.

199 Y. Li, R. Wang, H. Li, X. Wei, J. Feng, K. Liu, Y. Dang and A. Zhou, Efficient and stable photoelectrochemical seawater splitting with TiO_2@g-C_3N_4 nanorod arrays decorated by Co-Pi, *J. Phys. Chem. C*, 2015, **119**(35), 20283–20292.

200 Z. Liu and X. Lu, Multifarious function layers photoanode based on g-C_3N_4 for photoelectrochemical water splitting, *Chin. J. Catal.*, 2018, **39**(9), 1527–1533.

201 Y. Li, W. Shang, H. Li, M. Yang, S. Shi, J. Li, C. Huang and A. Zhou, Composite of Cobalt-C_3N_4 on TiO_2 Nanorod Arrays as Co-catalyst for Enhanced Photoelectrochemical Water Splitting, *ChemistrySelect*, 2021, **6**(17), 4319–4329.

202 A. K. Rathi, H. Kmentová, A. Naldoni, A. Goswami, M. B. Gawande, R. S. Varma, Š. Kment and R. Zbořil, Significant enhancement of photoactivity in hybrid TiO_2/g-C_3N_4 nanorod catalysts modified with Cu–Ni-based nanostructures, *ACS Appl. Nano Mater.*, 2018, **1**(6), 2526–2535.

203 W. Kong, X. Zhang, B. Chang, Y. Guo, Y. Li, S. Zhang and B. Yang, TiO_2 Nanorods Co-decorated with Metal-Free Carbon Materials for Boosted Photoelectrochemical Water Oxidation, *ChemElectroChem*, 2020, **7**(3), 792–799.

204 D. Chaudhary, S. Kumar and N. Khare, Boosting the visible-light photoelectrochemical performance of C_3N_4 by coupling with TiO_2 and carbon nanotubes: An organic/inorganic hybrid photocatalyst nanocomposite for photoelectrochemical water spitting, *Int. J. Hydrogen Energy*, 2020, **45**(55), 30091–30100.

205 Z. Yu, Y. Li, J. Qu, R. Zheng, J. M. Cairney, J. Zhang, M. Zhu, A. Khan and W. Li, Enhanced photoelectrochemical water-splitting performance with a hierarchical heterostructure: Co_3O_4 nanodots anchored TiO_2@ P-C_3N_4 core-shell nanorod arrays, *Chem. Eng. J.*, 2021, **404**, 126458.

206 Y. Liu, Y. X. Yu and W. D. Zhang, Photoelectrochemical study on charge transfer properties of nanostructured Fe_2O_3 modified by g-C_3N_4, *Int. J. Hydrogen Energy*, 2014, **39**(17), 9105–9113.

207 X. She, J. Wu, H. Xu, J. Zhong, Y. Wang, Y. Song and K. Nie, *et al.*, High efficiency photocatalytic water splitting using 2D α-Fe_2O_3/g-C_3N_4 Z-scheme catalysts. Advanced Energy, *Materials*, 2017, **7**(17), 1700025.

208 N. A. Arzaee, M. F. Mohamad Noh, N. S. H. M. Ita, N. A. Mohamed, S. N. Farhana Mohd Nasir, I. N. Nawas Mumthas, A. F. Ismail and M. A. Mat Teridi, Nanostructure-assisted charge transfer in α-Fe_2O_3/g-C_3N_4 heterojunctions for efficient and highly stable photoelectrochemical water splitting, *Dalton Trans.*, 2020, **49**(32), 11317–11328.

209 X. An, C. Hu, H. Lan, H. Liu and J. Qu, Strongly coupled metal oxide/reassembled carbon nitride/Co–Pi heterostructures

for efficient photoelectrochemical water splitting, *ACS Appl. Mater. Interfaces*, 2018, **10**(7), 6424–6432.

210 H. Tan, W. Peng, T. Zhang, Y. Han, L. Yin, W. Si, J. Liang and F. Hou, Highly polymerized wine-red carbon nitride to enhance photoelectrochemical water splitting performance of hematite, *J. Phys. Chem. C*, 2021, **125**(24), 13273–13282.

211 N. Bhandary, A. P. Singh, P. P. Ingole and S. Basu, Enhancing the photoelectrochemical performance of a hematite dendrite/graphitic carbon nitride nanocomposite through surface modification with CoFeOx, *ChemPhotoChem*, 2017, **1**(2), 70–75.

212 P. Arora, A. P. Singh, B. R. Mehta and S. Basu, Metal doped tubular carbon nitride (tC_3N_4) based hematite photoanode for enhanced photoelectrochemical performance, *Vacuum*, 2017, **146**, 570–577.

213 S. S. Yi, J. M. Yan and Q. Jiang, Carbon quantum dot sensitized integrated Fe_2O_3@g-C_3N_4 core–shell nanoarray photoanode towards highly efficient water oxidation, *J. Mater. Chem. A*, 2018, **6**(21), 9839–9845.

214 A. S. Reddy and J. Kim, An efficient g-C_3N_4-decorated CdS-nanoparticle-doped Fe_3O_4 hybrid catalyst for an enhanced H_2 evolution through photoelectrochemical water splitting, *Appl. Surf. Sci.*, 2020, **513**, 145836.

215 T. Annadurai, A. P. Khedulkar, J. Y. Lin, J. Adorna Jr, W. J. Yu, B. Pandit, T. V. Huynh and R. A. Doong, S-scheme N-doped carbon dots anchored g-C_3N_4/Fe_2O_3 shell/core composite for photoelectrocatalytic trimethoprim degradation and water splitting, *Appl. Catal., B*, 2023, **320**, 121928.

216 F. Zhan, R. Xie, W. Li, J. Li, Y. Yang, Y. Li and Q. Chen, *In situ* synthesis of g-C_3N_4/WO_3 heterojunction plates array films with enhanced photoelectrochemical performance, *RSC Adv.*, 2015, **5**(85), 69753–69760.

217 Y. Li, X. Wei, X. Yan, J. Cai, A. Zhou, M. Yang and K. Liu, Construction of inorganic–organic 2D/2D WO_3/g-C_3N_4 nanosheet arrays toward efficient photoelectrochemical splitting of natural seawater, *Phys. Chem. Chem. Phys.*, 2016, **18**(15), 10255–10261.

218 H. Li, F. Zhao, J. Zhang, L. Luo, X. Xiao, Y. Huang, H. Ji and Y. Tong, A g-C_3N_4/WO_3 photoanode with exceptional ability for photoelectrochemical water splitting, *Mater. Chem. Front.*, 2017, **1**(2), 338–342.

219 J. Xiao, X. Zhang and Y. Li, A ternary g-C_3N_4/Pt/ZnO photoanode for efficient photoelectrochemical water splitting, *Int. J. Hydrogen Energy*, 2015, **40**(30), 9080–9087.

220 T. J. Park, R. C. Pawar, S. Kang and C. S. Lee, Ultra-thin coating of g-C3N4 on an aligned ZnO nanorod film for rapid charge separation and improved photodegradation performance, *RSC Adv.*, 2016, **6**(92), 89944–89952.

221 C. Liu, Y. Qiu, F. Wang, K. Wang, Q. Liang and Z. Chen, Design of core–shell-structured ZnO/ZnS hybridized with graphite-like C_3N_4 for highly efficient photoelectrochemical water splitting, *Adv. Mater. Interfaces*, 2017, **4**(21), 1700681.

222 Š. Hajduk, S. P. Berglund, M. Podlogar, G. Dražić, F. F. Abdi and Z. C. Orel, and M. Shalom. Conformal Carbon Nitride Coating as an Efficient Hole Extraction Layer for ZnO Nanowires-Based Photoelectrochemical Cells, *Adv. Mater. Interfaces*, 2017, **4**(24), 1700924.

223 C. Mahala, M. D. Sharma and M. Basu, ZnO nanosheets decorated with graphite-like carbon nitride quantum dots as photoanodes in photoelectrochemical water splitting, *ACS Appl. Nano Mater.*, 2020, **3**(2), 1999–2007.

224 C. Liu, P. Wu, K. Wu, G. Meng, J. Wu, J. Hou, Z. Liu and X. Guo, Advanced bi-functional CoPi co-catalyst-decorated g-C_3N_4 nanosheets coupled with ZnO nanorod arrays as integrated photoanodes, *Dalton Trans.*, 2018, **47**(18), 6605–6614.

225 M. Sun, Z. Chen, X. Jiang, C. Feng and R. Zeng, Optimized preparation of Co-Pi decorated g-C3N4@ ZnO shell-core nanorod array for its improved photoelectrochemical performance and stability, *J. Alloys Compd.*, 2019, **780**, 540–551.

226 C. Liu, Y. Qiu, J. Zhang, Q. Liang, N. Mitsuzaki and Z. Chen, Construction of CdS quantum dots modified g-C3N4/ZnO heterostructured photoanode for efficient photoelectrochemical water splitting, *J. Photochem. Photobiol., A*, 2019, **371**, 109–117.

227 Z. Masoumi, M. Tayebi, M. Kolaei and B. K. Lee, Improvement of surface light absorption of ZnO photoanode using a double heterojunction with α–Fe_2O_3/g–C_3N_4 composite to enhance photoelectrochemical water splitting, *Appl. Surf. Sci.*, 2023, **608**, 154915.

228 H. Bian, A. Wang, Z. Li, Z. Li, Y. Diao, J. Lu and Y. Y. Li, g-C_3N_4-Modified Water-Crystallized Mesoporous SnO2 for Enhanced Photoelectrochemical Properties, *Part. Part. Syst. Charact.*, 2018, **35**(10), 1800155.

229 B. Babu, R. Koutavarapu, J. Shim and K. Yoo, Enhanced visible-light-driven photoelectrochemical and photocatalytic performance of Au-SnO_2 quantum dot-anchored g-C_3N_4 nanosheets, *Sep. Purif. Technol.*, 2020, **240**, 116652.

230 P. Chaudhary and P. P. Ingole, In-Situ solid-state synthesis of 2D/2D interface between Ni/NiO hexagonal nanosheets supported on g-C_3N_4 for enhanced photo-electrochemical water splitting, *Int. J. Hydrogen Energy*, 2020, **45**(32), 16060–16070.

231 U. Baig, A. Khan, M. A. Gondal, M. A. Dastageer and W. S. Falath, Laser induced anchoring of nickel oxide nanoparticles on polymeric graphitic carbon nitride sheets using pulsed laser ablation for efficient water splitting under visible light, *Nanomaterials*, 2020, **10**(6), 1098.

232 H. Hao, D. Lu and Q. Wang, Photoelectrochemical study on charge separation mechanisms of Bi_2WO_6 quantum dots decorated g-C_3N_4, *Int. J. Hydrogen Energy*, 2018, **43**(18), 8824–8834.

233 C. Murugan, K. Ranjithkumar and A. Pandikumar, Interfacial charge dynamics in type-II heterostructured sulfur doped-graphitic carbon nitride/bismuth tungstate as competent photoelectrocatalytic water splitting photoanode, *J. Colloid Interface Sci.*, 2021, **602**, 437–451.

234 Y. Wang, Y. Tian, L. Yan and Z. Su, DFT study on sulfur-doped g-C_3N_4 nanosheets as a photocatalyst for CO_2 reduction reaction, *J. Phys. Chem. C*, 2018, **122**(14), 7712–7719.

235 C. V. Reddy, R. Koutavarapu, I. N. Reddy and J. Shim, Effect of a novel one-dimensional zinc tungsten oxide nanorods anchored two-dimensional graphitic carbon nitride nanosheets for improved solar-light-driven photocatalytic removal of toxic pollutants and photoelectrochemical water splitting, *J. Mater. Sci.: Mater. Electron.*, 2021, **32**, 33–46.

236 C. Murugan, R. A. Nataraj, M. P. Kumar, S. Ravichandran and A. Pandikumar, Enhanced Charge Transfer Process of Bismuth Vanadate Interleaved Graphitic Carbon Nitride Nanohybrids in Mediator-Free Direct Z Scheme Photoelectrocatalytic Water Splitting, *ChemistrySelect*, 2019, **4**(16), 4653–4663.

237 P. Mane, H. Bae, V. Burungale, S. W. Lee, M. Misra, H. Parbat, A. N. Kadam and J. S. Ha, Interface-engineered Z-scheme of $BiVO_4$/g-C_3N_4 photoanode for boosted photoelectrochemical water splitting and organic contaminant elimination under solar light, *Chemosphere*, 2022, **308**, 136166.

238 M. F. R. Samsudin, H. Ullah, R. Bashiri, N. M. Mohamed, S. Sufian and Y. H. Ng, Experimental and DFT insights on microflower g-C3N4/BiVO4 photocatalyst for enhanced photoelectrochemical hydrogen generation from lake water, *ACS Sustainable Chem. Eng.*, 2020, **8**(25), 9393–9403.

239 B. Zhang, S. Y. Zhao, H. H. Wang, T. J. Zhao, Y. X. Liu, L. B. Lv, X. Wei, X. H. Li and J. S. Chen, The solution-phase process of a g-C_3N_4/$BiVO_4$ dyad to a large-area photoanode: interfacial synergy for highly efficient water oxidation, *Chem. Commun.*, 2017, **53**(76), 10544–10547.

240 C. Feng, Z. Wang, Y. Ma, Y. Zhang, L. Wang and Y. Bi, Ultrathin graphitic C_3N_4 nanosheets as highly efficient metal-free cocatalyst for water oxidation, *Appl. Catal., B*, 2017, **205**, 19–23.

241 G. Zeng, X. Wang, X. Yu, J. Guo, Y. Zhu and Y. Zhang, Ultrathin g-C_3N_4/Mo:$BiVO_4$ photoanode for enhanced photoelectrochemical water oxidation, *J. Power Sources*, 2019, **444**, 227300.

242 K. H. Ye, H. Li, D. Huang, S. Xiao, W. Qiu, M. Li, Y. Hu, W. Mai, H. Ji and S. Yang, Enhancing photoelectrochemical water splitting by combining work function tuning and heterojunction engineering, *Nat. Commun.*, 2019, **10**(1), 3687.

243 N. A. Mohamed, H. Ullah, J. Safaei, A. F. Ismail, M. F. Mohamad Noh, M. F. Soh, M. A. Ibrahim, N. A. Ludin and M. A. Mat Teridi, Efficient photoelectrochemical performance of γ irradiated g-C_3N_4 and its g-C_3N_4 @ BiVO4 heterojunction for solar water splitting, *J. Phys. Chem. C*, 2019, **123**(14), 9013–9026.

244 T. Jiang, F. Nan, J. Zhou, F. Zheng, Y. Weng, T. Y. Cai, S. Ju, B. Xu and L. Fang, Enhanced photocatalytic and photoelectrochemical performance of g-C3N4/BiVO4 heterojunction: A combined experimental and theoretical study, *AIP Adv.*, 2019, **9**(5), 055225.

245 J. Prakash, U. Prasad, R. Alexander, J. Bahadur, K. Dasgupta and A. N. Mada Kannan, Photoelectrochemical solar water splitting: the role of the carbon nanomaterials in bismuth vanadate composite photoanodes toward efficient charge separation and transport, *Langmuir*, 2019, **35**(45), 14492–14504.

246 D. Sariket, D. Ray, S. Baduri, S. Ghosh, A. Maity and C. Bhattacharya, Synthesis of g-C_3N_4/$InVO_4$ Semiconductor for Improved Photocatalytic and Photoelectrochemical Applications, *Electroanalysis*, 2020, **32**(11), 2535–2544.

247 Y. Li, G. Liu, D. Jia, C. Li, L. Wang, J. Zheng, X. Liu and Z. Jiao, Nanoporous $FeVO_4$ Photoanodes Modified with Ultrathin C_3N_4 for High Photoelectrochemical Water Splitting Performance, *Catal. Lett.*, 2019, **149**, 19–24.

248 Y. Cao, Roadmap and direction toward high-performance MoS_2 hydrogen evolution catalysts, *ACS Nano*, 2021, **15**(7), 11014–11039.

249 X. Hu, X. Zeng, Y. Liu, J. Lu, S. Yuan, Y. Yin, J. Hu, D. T. McCarthy and X. Zhang, Nano-layer based 1T-rich MoS2/g-C3N4 co-catalyst system for enhanced photocatalytic and photoelectrochemical activity, *Appl. Catal., B*, 2020, **268**, 118466.

250 L. Ge, C. Han, X. Xiao and L. Guo, Synthesis and characterization of composite visible light active photocatalysts MoS_2–g-C_3N_4 with enhanced hydrogen evolution activity, *Int. J. Hydrogen Energy*, 2013, **38**(17), 6960–6969.

251 L. Ye, D. Wang and S. Chen, Fabrication and enhanced photoelectrochemical performance of MoS_2/S-doped g-C_3N_4 heterojunction film, *ACS Appl. Mater. Interfaces*, 2016, **8**(8), 5280–5289.

252 L. Ye, H. Zhang, Y. Xiong, C. Kong, H. Li and W. Li, Efficient photoelectrochemical overall water-splitting of MoS_2/g-C_3N_4 n–n type heterojunction film, *J. Chem. Phys.*, 2021, **154**(21), 214701.

253 P. Subramanyam, B. Meena, D. Suryakala, M. Deepa and C. Subrahmanyam, Plasmonic nanometal decorated photoanodes for efficient photoelectrochemical water splitting, *Catal. Today*, 2021, **379**, 1–6.

254 S. B. Kokane, R. Sasikala, D. M. Phase and S. D. Sartale, In_2S_3 nanoparticles dispersed on g-C_3N_4 nanosheets: role of heterojunctions in photoinduced charge transfer and photoelectrochemical and photocatalytic performance, *J. Mater. Sci.*, 2017, **52**, 7077–7090.

255 M. D. Sharma and M. Basu, Nanosheets of In_2S_3/S- C_3N_4 -Dots for Solar Water-Splitting in Saline Water, *Langmuir*, 2022, **38**(42), 12981–12990.

256 R. Wang, J. Yan, M. Zu, S. Yang, X. Cai, Q. Gao, Y. Fang, S. Zhang and S. Zhang, Facile synthesis of interlocking g-C_3N_4/CdS photoanode for stable photoelectrochemical hydrogen production, *Electrochim. Acta*, 2018, **279**, 74–83.

257 T. Mahvelati-Shamsabadi, E. K. Goharshadi and M. Karimi-Nazarabad, Z-scheme design of Ag@g- C_3N_4/ZnS photoanode device for efficient solar water oxidation: An organic-inorganic electronic interface, *Int. J. Hydrogen Energy*, 2019, **44**(26), 13085–13097.

258 C. He, J. H. Zhang, W. X. Zhang and T. T. Li, Type-II InSe/g-C_3N_4 heterostructure as a high-efficiency oxygen evolution reaction catalyst for photoelectrochemical water splitting, *J. Phys. Chem. Lett.*, 2019, **10**(11), 3122–3128.

259 S. J. Kim, Y. Lee, D. K. Lee, J. W. Lee and J. K. Kang, Efficient Co–Fe layered double hydroxide photocatalysts for water oxidation under visible light, *J. Mater. Chem. A*, 2014, **2**(12), 4136–4139.

260 W. Lin and H. Frei, Photochemical CO_2 splitting by metal-to-metal charge-transfer excitation in mesoporous ZrCu (I)-MCM-41 silicate sieve, *J. Am. Chem. Soc.*, 2005, **127**(6), 1610–1611.

261 Y. Hou, Z. Wen, S. Cui, X. Feng and J. Chen, Strongly coupled ternary hybrid aerogels of N-deficient porous graphitic-C_3N_4 nanosheets/N-doped graphene/NiFe-layered double hydroxide for solar-driven photoelectrochemical water oxidation, *Nano Lett.*, 2016, **16**(4), 2268–2277.

262 M. Arif, G. Yasin, M. Shakeel, X. Fang, R. Gao, S. Ji and D. Yan, Coupling of bifunctional CoMn-layered double hydroxide@graphitic C_3N_4 nanohybrids towards efficient photoelectrochemical overall water splitting, *Chem. – Asian J.*, 2018, **13**(8), 1045–1052.

263 M. Arif, G. Yasin, M. Shakeel, M. A. Mushtaq, W. Ye, X. Fang, S. Ji and D. Yan, Hierarchical CoFe-layered double hydroxide and g-C_3N_4 heterostructures with enhanced bifunctional photo/electrocatalytic activity towards overall water splitting, *Mater. Chem. Front.*, 2019, **3**(3), 520–531.

264 X. Fan, T. Wang, B. Gao, X. Xie, S. Zhang, X. Meng, H. Gong, Y. Guo, X. Huang and J. He, Layered double hydroxides decorated graphic carbon nitride film as efficient photoanodes for photoelectrochemical water splitting, *Catal. Today*, 2019, **335**, 423–428.

265 S. Nayak and K. M. Parida, Deciphering Z-scheme charge transfer dynamics in heterostructure NiFe-LDH/N-rGO/g-C_3N_4 nanocomposite for photocatalytic pollutant removal and water splitting reactions, *Sci. Rep.*, 2019, **9**(1), 2458.

266 S. Guru, S. Kumar, S. Bellamkonda and R. R. Gangavarapu, Synthesis of CuTi-LDH supported on g-C_3N_4 for electrochemical and photoelectrochemical oxygen evolution reactions, *Int. J. Hydrogen Energy*, 2021, **46**(30), 16414–16430.

267 S. Guru, Bismuth oxycarbonate grafted NiFe-LDH supported on g-C_3N_4 as bifunctional catalyst for photoelectrochemical water splitting, *Int. J. Hydrogen Energy*, 2021, **46**(22), 12145–12157.

268 K. N. Mahdi, E. K. Goharshadi and H. S. Sajjadizadeh, Copper–Azolate Framework Coated on g-C_3N_4 Nanosheets as a Core–Shell Heterojunction and Decorated with a $Ni(OH)_2$ Cocatalyst for Efficient Photoelectrochemical Water Splitting, *J. Phys. Chem. C*, 2022, **126**(19), 8327–8336.

269 R. Cao, H. Yang, S. Zhang and X. Xu, Engineering of Z-scheme 2D/3D architectures with $Ni(OH)_2$ on 3D porous g-C_3N_4 for efficiently photocatalytic H2 evolution, *Appl. Catal., B*, 2019, **258**, 117997.

270 V. Selvaraj and A. Pandikumar, Turning UV light-active BiOF into visible light-active BiOF by forming a heterojunction with g-C_3N_4 and its photoelectrochemical water splitting performance in reverse osmosis-rejected wastewater, *J. Phys. Chem. C*, 2021, **126**(1), 79–90.

271 S. Vinoth, P. M. Rajaitha and A. Pandikumar, Modulating photoelectrochemical water splitting performance by constructing a type-II heterojunction between g-C_3N_4 and BiOI, *New J. Chem.*, 2021, **45**(4), 2010–2018.

272 P. Velusamy, X. Liu, M. Sathiya, N. S. Alsaiari, F. M. Alzahrani, M. T. Nazir, E. Elamurugu, M. Senthil Pandian and F. Zhang, Investigate the suitability of g-C_3N_4 nanosheets ornamented with BiOI nanoflowers for photocatalytic dye degradation and PEC water splitting, *Chemosphere*, 2023, 138007.

273 P. Velusamy, M. Sathiya, Y. Liu, S. Liu, R. Ramesh Babu, M. A. Saad Aly, E. Elangovan, H. Chang, L. Mao and R. Xing, Investigating the effect of Nd^{3+} dopant and the formation of g-C_3N_4/BiOI heterostructure on the microstructural, optical and photoelectrocatalytic properties of g-C3N4, *Appl. Surf. Sci.*, 2021, **561**, 150082.

274 Y. Ma, Z. Wang, Y. Jia, L. Wang, M. Yang, Y. Qi and Y. Bi, Bi_2MoO_6 nanosheet array modified with ultrathin graphitic carbon nitride for high photoelectrochemical performance, *Carbon*, 2017, **114**, 591–600.

275 J. Li, H. Yuan and Z. Zhu, Improved photoelectrochemical performance of Z-scheme g-C_3N_4/Bi_2O_3/$BiPO_4$ heterostructure and degradation property, *Appl. Surf. Sci.*, 2016, **385**, 34–41.

276 N. A. Mohamed, A. F. Ismail, J. Safaei, M. R. Johan and M. A. Mat Teridi, A novel photoanode based on Thorium oxide (ThO_2) incorporated with graphitic Carbon nitride (g-C_3N_4) for Photoelectrochemical water splitting, *Appl. Surf. Sci.*, 2021, **569**, 151043.

277 Y. Zheng, Q. Ruan, J. X. Ren, X. Guo, Y. Zhou, B. Zhou, Q. Xu, Q. Fu, S. Wang and Y. Huang, Plasma-assisted liquid-based growth of g-C_3N_4/Mn_2O_3 pn heterojunction with tunable valence band for photoelectrochemical application, *Appl. Catal., B*, 2023, **323**, 122170.

278 N. Bhandary, A. P. Singh, S. Kumar, P. P. Ingole, G. S. Thakur, A. K. Ganguli and S. Basu, In situ solid-state synthesis of a AgNi/g-C_3N_4 nanocomposite for enhanced photoelectrochemical and photocatalytic activity, *ChemSusChem*, 2016, **9**(19), 2816–2823.

279 Z. Chen, G. Ma, Z. Chen, Y. Zhang, Z. Zhang, J. Gao and Q. Meng, *et al.*, Fabrication and photoelectrochemical properties of silicon nanowires/g-C_3N_4 core/shell arrays, *Appl. Surf. Sci.*, 2017, **396**, 609–615.

280 U. Baig, A. Khan, M. A. Gondal, M. A. Dastageer and S. Akhtar, Single-step synthesis of silicon carbide anchored graphitic carbon nitride nanocomposite photo-catalyst for efficient photoelectrochemical water splitting under visible-light irradiation, *Colloids Surf., A*, 2021, **611**, 125886.

281 Z. Huang, X. Zeng, K. Li, S. Gao, Q. Wang and J. Lu, Z-scheme $NiTiO_3$/g-C_3N_4 heterojunctions with enhanced photoelectrochemical and photocatalytic performances under visible LED light irradiation, *ACS Appl. Mater. Interfaces*, 2017, **9**(47), 41120–41125.

282 Y. Liu, J. Zhang, X. Li, Z. Yao, L. Zhou, H. Sun and S. Wang, Graphitic carbon nitride decorated with CoP nanocrystals for enhanced photocatalytic and photoelectrochemical H_2 evolution, *Energy Fuels*, 2019, **33**(11), 11663–11676.

283 Y. Liu, X. Li, H. He, S. Yang, G. Jia and S. Liu, CoP imbedded g-C_3N_4 heterojunctions for highly efficient

photo, electro and photoelectrochemical water splitting, *J. Colloid Interface Sci.*, 2021, **599**, 23–33.

284 M. M. Islam, R. D. Tentu and S. Basu, Synthesis of g-C_3N_4/$ZnGa_{1.9}Al_{0.1}O_4$ Heterojunction Using Narrow and Wide Band Gap Material for Enhanced Photoelectrochemical Water Splitting, *ChemistrySelect*, 2018, **3**(2), 486–494.

285 J. Hou, H. Cheng, O. Takeda and H. Zhu, Unique 3D heterojunction photoanode design to harness charge transfer for efficient and stable photoelectrochemical water splitting, *Energy Environ. Sci.*, 2015, **8**(4), 1348–1357.

286 X. Xu, Y. Liu, Y. Zhu, X. Fan, Y. Li, F. Zhang, G. Zhang and W. Peng, Fabrication of a Cu_2O/g-C_3N_4/WS_2 Triple-Layer Photocathode for Photoelectrochemical Hydrogen Evolution, *ChemElectroChem*, 2017, **4**(6), 1498–1502.

287 X. Ma, J. Zhang, B. Wang, Q. Li and S. Chu, Hierarchical Cu_2O foam/g-C_3N_4 photocathode for photoelectrochemical hydrogen production, *Appl. Surf. Sci.*, 2018, **427**, 907–916.

288 R. S. Moakhar, F. Soleimani, S. K. Sadrnezhaad, S. Masudy-Panah, R. Katal, A. Seza, N. Ghane and S. Ramakrishna, One-pot microwave synthesis of hierarchical C-doped CuO dandelions/g-C_3N_4 nanocomposite with enhanced photostability for photoelectrochemical water splitting, *Appl. Surf. Sci.*, 2020, **530**, 147271.

289 V. Ragupathi, M. A. Raja, P. Panigrahi and N. G. Subramaniam, CuO/g-C_3N_4 nanocomposite as promising photocatalyst for photoelectrochemical water splitting, *Optik*, 2020, **208**, 164569.

290 Q. Huang, Z. Ye and X. Xiao, Recent progress in photocathodes for hydrogen evolution, *J. Mater. Chem. A*, 2015, **3**(31), 15824–15837.

291 P. P. Kunturu and J. Huskens, Improving Charge Separation in Cu_2O/g-C_3N_4/CoS Photocathodes by a Z-Scheme Heterojunction to Achieve Enhanced Performance and Photostability, *Clean Energy Materials*, American Chemical Society, 2020, pp. 111–136.

292 F. Yang, V. Kuznietsov, M. Lublow, C. Merschjann, A. Steigert, J. Klaer, A. Thomas and T. Schedel-Niedrig, Solar hydrogen evolution using metal-free photocatalytic polymeric carbon nitride/$CuInS_2$ composites as photocathodes, *J. Mater. Chem. A*, 2013, **1**(21), 6407–6415.

293 D. Wang, C. Wang, F. P. Garcia de Arquer, J. Zhong, L. Qian, L. Fang and P. Liu, *et al.*, Band-aligned C_3N_4−$xS_{3x/2}$ stabilizes CdS/$CuInGaS_2$ photocathodes for efficient water reduction, *J. Mater. Chem. A*, 2017, **5**(7), 3167–3171.

294 Z. Wang, B. Jin, G. Zou, K. Zhang, X. Hu and J. H. Park, Rationally Designed Copper-Modified Polymeric Carbon Nitride as a Photocathode for Solar Water Splitting, *ChemSusChem*, 2019, **12**(4), 866–872.

295 Y. Zhang, Z. Schnepp, J. Cao, S. Ouyang, Y. Li, J. Ye and S. Liu, Biopolymer-activated graphitic carbon nitride towards a sustainable photocathode material, *Sci. Rep.*, 2013, **3**(1), 2163.

296 J. Wang, F. Y. Su and W. D. Zhang, Preparation and enhanced visible light photoelectrochemical activity of g-C_3N_4/ZnO nanotube arrays, *J. Solid State Electrochem.*, 2014, **18**, 2921–2929.

297 Y. Dong, Y. Chen, P. Jiang, G. Wang, X. Wu and R. Wu, A novel g-C_3N_4 based photocathode for photoelectrochemical hydrogen evolution, *RSC Adv.*, 2016, **6**(9), 7465–7473.

298 M.-Y. Ye, Z.-H. Zhao, Z.-F. Hu, L.-Q. Liu, H.-M. Ji, Z.-R. Shen and T.-Y. Ma, 0D/2D heterojunctions of vanadate quantum dots/graphitic carbon nitride nanosheets for enhanced visible-light-driven photocatalysis, *Angew. Chem., Int. Ed.*, 2017, **56**(29), 8407–8411.

299 G. S. Shanker, R. Bhosale, S. Ogale and A. Nag, 2D Nanocomposite of g-C_3N_4 and TiN Embedded N-Doped Graphene for Photoelectrochemical Reduction of Water Using Sunlight, *Adv. Mater. Interfaces*, 2018, **5**(24), 1801488.

300 Y.-Y. Han, X.-L. Lu, S.-F. Tang, X.-P. Yin, Z.-W. Wei and T.-B. Lu, Metal-free 2D/2D heterojunction of graphitic carbon nitride/graphdiyne for improving the hole mobility of graphitic carbon nitride. Advanced Energy, *Materials*, 2018, **8**(16), 1702992.

301 S. Gopalakrishnan, G. M. Bhalerao and K. Jeganathan, $SrTiO_3$ NPs/g-C_3N_4 NSs coupled Si NWs based hybrid photocathode for visible light driven photoelectrochemical water reduction, *ACS Sustainable Chem. Eng.*, 2019, **7**(16), 13911–13919.

302 G. S. Shanker, R. A. Panchal, S. Ogale and A. Nag, g-C_3N_4: Sn-doped In_2O_3 (ITO) nanocomposite for photoelectrochemical reduction of water using solar light, *J. Solid State Chem.*, 2020, **285**, 121187.

303 S. Wang, F. Nan, Y. Zhou, F. Zheng, Y. Weng, L. You and L. Fang, Enhanced photoelectrochemical performance in $BiFeO_3$/g-C_3N_4 p–n heterojunction photocathodes with ferroelectric polarization, *J. Appl. Phys.*, 2020, **128**(15), 154101.

304 S. Wang, F. Zheng, Y. Weng, G. Yuan, L. Fang and L. You, Enhanced Photoelectrochemical Performance by Interface Engineering in Ternary g-C_3N_4/TiO_2/$PbTiO_3$ Films, *Adv. Mater. Interfaces*, 2020, **7**(10), 2000185.

305 V. Guigoz, L. Balan, A. Aboulaich, R. Schneider and T. Gries, Heterostructured thin $LaFeO_3$/g-C_3N_4 films for efficient photoelectrochemical hydrogen evolution, *Int. J. Hydrogen Energy*, 2020, **45**(35), 17468–17479.

306 E. Sitara, H. Nasir, A. Mumtaz, M. F. Ehsan, M. Sohail, S. Iram, S. A. Batool Bukhari, S. Ullah, T. Akhtar and A. Iqbal, Enhanced photoelectrochemical water splitting using zinc selenide/graphitic carbon nitride type-II heterojunction interface, *Int. J. Hydrogen Energy*, 2021, **46**(50), 25424–25435.

307 P. Babu, H. Kim, J. Y. Park and B. Naik, Trioctylphosphine Oxide (TOPO)-Assisted Facile Fabrication of Phosphorus-Incorporated Nanostructured Carbon Nitride Toward Photoelectrochemical Water Splitting with Enhanced Activity, *Inorg. Chem.*, 2022, **61**(3), 1368–1376.